# Review of Experiments that Contradict Special Relativity and Support neo-Lorentz Relativity: Latest Technique to Detect Dynamical Space Using Quantum Detectors

**Reginald T. Cahill**
School of Chemical and Physical Sciences, Flinders University, Adelaide 5001, Australia
April 2015
NPA 2014 Baltimore Conference

The anisotropy of the velocity of EM radiation has been repeatedly detected, including the Michelson-Morley experiment of 1887, using a variety of techniques. The experiments reveal the existence of a dynamical space that has a velocity of some 500km/s from a southerly direction. These consistent experiments contradict the assumptions of Special Relativity, but are consistent with the assumptions of neo-Lorentz Relativity. The existence of the dynamical space has been missed by physics since its beginnings. Novel and checkable phenomena then follow from including this space in Quantum Theory, EM Theory, Cosmology, etc, including the derivation of a more general theory of gravity as a quantum wave refraction effect. The corrected Schrödinger equation has resulted in a very simple and robust quantum detector, which easily measures the speed and direction of the dynamical space. This report reviews the key experimental evidence.



## 1 Introduction

Determining the nature of reality, in the sense of discovering the properties of space, time, matter, has been a longstanding problem since the time of the ancient greek physicists, who argued, theoretically, long and deeply and without agreement. With the discovery by Galileo that experiment was the missing key aspect of the scientific method, progress appeared to speed up. Galileo introduced geometrical models for space and time, which were adopted by Newton, and which persisted until the most famous of all experiments by Michelson and Morley in 1887. That experiment was conceived as a technique to determine the velocity of the earth through the aether, a substance that supposedly filled Galileo's geometrical space. Almost all physics publications assert that this interferometer experiment produced a null result, namely that on rotation the fringe shifts did not move, which would have been the case if an aether was flowing past the device, and for which the speed of light was fixed relative to the aether. This putative null result was used by Einstein in 1905 to initiate a new theory for space and time, namely that space and time were not separate phenomena, but were united into space-time, in which there is no observer independent notion of space or time, and no aether. This space-time model has persisted until the present time, and has completely determined the understanding of reality by academic physicists. However the Michelson-Morley 1887 paper [33] reveals observed fringe shifts and a speed of up to 10km/s. which was less than expected. But the key point is that they used Galilean-Newtonian physics to calibrate the interferometer, which provided the computation from the observed fringe shifts to a speed of translation of the earth. So the data was indicating the failure of that calibration theory, and not that the results amounted to a null effect. Another mistake by MM was to average data from different days, but at the same local solar time. So MM missed the discovery also of gravitational waves, for which the averaging washed out the wave effects. However in 2002 Cahill and Kitto [5, 7] used Lorentz relativity to recalibrate the sensitivity of the MM detector. It was then discovered that the Michelson interferometer had a fundamental design flaw, that had gone unnoticed since 1887, namely that the device had zero sensitivity unless operated with a dielectric present in the light paths. Indeed the 1887 experiment had air present, and the new calibration theory im-

plied that it was some 2000 times less sensitive than assumed by MM. Some of MM 1887 data is shown in Fig.3, together with some data from the 1925/26 Miller [34] interferometer experiment. So the staring point for Einstein's spacetime model, whose key assumption is that the speed of light is the same in all directions and for all observers, is contradicted by the earliest experiment. All Michelson interferometer experiments in recent years use vacuum mode, and so have zero sensitivity to light speed anisotropy. So some 100 years after Einstein's innovation of 'spacetime', it has been necessary to review all relevant experiments, to develop new experimental techniques, and to rebuild the foundations of physics. The new foundations involve a dynamical space, with no aether, and this theory has been tested against data from numerous experiments and earth and astronomical observations. A key development has been the discovery of a new theory of gravity, namely that it is caused by quantum matter waves being refracted by inhomogeneities and time dependencies of the velocity field that describes the dynamical space. Until recently all experiments to detect and characterise the dynamical space have used either light speed or RF EM wave speed anisotropies. However in 2013 a quantum effect was discovered, in which the passing dynamical space modifies the current through a reverse-biased Zener diode Cahill [23]. This has made the determination of the flow of space essentially very cheap, simple and robust. The observed fluctuations are actual gravitational waves, but not with the characteristics predicted by General Relativity, which have never been detected. All the non-null experimental data from 1887 to 2014 now agree wrt the speed and direction of the earth through the dynamical space, and only some of that data is reviewed here. As well new phenomena caused by the fluctuations in the flow of space are now being discovered. The most significant is that the dynamical space does not have a measure of energy, but can induce energy in matter systems. This means that the Conservation of Energy Principle, namely the 1st Law of Thermodynamics, does not apply to space-flow turbulence/gravitational-wave induced effects [27, 28].

## 2 Relativity Theories

A "Relativity Principle" (RP) specifies how observations by different observers are related. In doing so the RP reflects fundamental aspects of realty, and any proposed RP is subject to ongoing experimental challenge.

There have been three major relativity theories: Galileo Relativity (GaR), Lorentz Relativity (LR) and Einstein Special Relativity (SR), with the later much celebrated, while the LR is essentially ignored. Yet it is often incorrectly claimed that LR and SR are experimentally indistinguishable. It has been shown [13, 26] that (i) they are experimentally distinguishable, (ii) that comparison of gas-mode Michelson interferometer experiments with spacecraft earth-flyby Doppler shift data [16] demonstrate that it is LR that is consistent with the data, while SR is in conflict with the same data, (iii) SR is exactly derivable from Galilean Relativity by means of change of space and time coordinates, so that the well-known SR relativistic effects are purely coordinate effects, and cannot correspond to the observed dynamical relativistic effects. The connections between these three relativity theories has become apparent following the discovery that space is a dynamical and observable system, and that space and time are distinct phenomena.

We give a non-historical presentation, because historical presentations were always confused by the lack of realisation that a dynamical space existed, although serious consideration was given to Lorentz Relativity [2–4].

But 1st a warning: a common error when discussing the physics of space and time is to confuse space and time coordinates with the actual phenomenon of space and time, and also to confuse space intervals, as measured by a ruler or round trip light speed measurements, and time measured by an actual clock, with actual intrinsic measures of space and time phenomena: coordinates are arbitrary, whereas the intrinsic measures are set by the dynamics of space.

## 3 Galilean Relativity

We give here a modern statement of Galilean Relativity. The assumptions in GaR are (i) space exists, but is not observable and not dynamical, and is modelled as a Euclidean 3-space ($E^3$), which entails the notion that space is without structure, (ii) observers measure space and time intervals using rods and clocks, whose respective lengths and time intervals are not affected by their motion through space, (iii) the speed of light (in vacuum) is fixed at $c$ wrt the space, and (iv) velocities are measured relative to observers, where different observers, $O$ and $O'$, relate their space and time coordinates by

$$t' = t, \quad x' = x - Vt, \quad y' = y, \quad z' = z. \tag{1}$$

where $V$ is the relative speed of the observers (in their common $x$-direction, for simplicity). The speed $w$ of an object or waveform (in the $x$ direction) according to each observer, is related by

$$w' = w - V \tag{2}$$

Eqns (1) and (2) form the Galilean Relativity Transformation, and the underlying assumptions define Galilean Relativity (GaR). Newton based his dynamics on Galilean Relativity, in particular his theory of gravity, to which General Relativity reduces in the limit of low mass densities and low speeds.

# 4 Lorentz and Neo-Lorentz Relativity

When Maxwell formulated his unification of electric and magnetic fields* the speed of EM waves came out to be the constant $c = 1/\sqrt{\epsilon_0 \mu_0}$ for any observer, and so independent of the motion of the observers wrt one another or to space. This overtly contradicted GaR, in (2). Hertz in 1890 [29] pointed out the obvious fix-up, namely that Maxwell had mistakenly not used the then-known Euler constituent derivative $\partial/\partial t + \mathbf{v} \cdot \nabla$, in place of $\partial/\partial t$, where $\mathbf{v}$ is the velocity of some structure to space relative to an observer, in which case Maxwell's equations would only be valid in the local rest frame defined by this structure. In that era a dual model was then considered, namely with a Euclidean space $E^3$ and an extended all-filling aether substance, so that the velocity $\mathbf{v}$ was the velocity of the aether relative to an observer. To be explicit let us consider the case of electromagnetic waves, as described by the vector potential $\mathbf{A}(\mathbf{r}, t)$ satisfying the wave equation (in absence of charges and currents), but using the Euler constituent derivative, as suggested by Hertz:

$$\left(\frac{\partial}{\partial t} + \mathbf{v}(\mathbf{r}, t) \cdot \nabla\right)^2 \mathbf{A}(\mathbf{r}, t) = c^2 \nabla^2 \mathbf{A}(\mathbf{r}, t). \qquad (3)$$

Here $\nabla = \{\frac{\partial}{\partial x}, \frac{\partial}{\partial y}, \frac{\partial}{\partial z}\}$. In Lorentz Relativity there is an aether in addition to an actual Euclidean space, and $\mathbf{v}$ is independent of $\mathbf{r}$ and $t$; whereas in neo-Lorentz Relativity $\mathbf{v}(\mathbf{r}, t)$ describes a dynamical space, with $\mathbf{r}$ and $t$ describing a coordinate system for space and time. We find plane-wave solutions only for the case where the space flow velocity, relative to an observer, is locally time and space independent, *viz* uniform,

$$\mathbf{A}(\mathbf{r}, t) = \mathbf{A}_0 \sin(\mathbf{k} \cdot \mathbf{r} - \omega t)$$

with $\omega(\mathbf{k}, \mathbf{v}) = c|\vec{\mathbf{k}}| + \mathbf{v} \cdot \mathbf{k}$. The EM wave group velocity is then

$$\mathbf{v}_g = \vec{\nabla}_k \omega(\mathbf{k}, \mathbf{v}) = c\hat{\mathbf{k}} + \mathbf{v}$$

and we see that the wave has velocity $\mathbf{v}_g$ relative to the observer, with the space flowing at velocity $\mathbf{v}$ also relative to the observer, and so the EM speed is $c$ in direction $\hat{\mathbf{k}}$ relative to the aether (LR) or dynamical space (nLR). In searching for experimental evidence for the existence of this aether, or more generally a Preferred Frame of Reference (PFR), Michelson conceived of his interferometer [33]. Unknown to Michelson was that his design had an intrinsic fatal flaw: if operated in vacuum mode it was incapable of detecting the PFR effect, while with air present, as operated by Michelson and Morley in 1887, it was extremely insensitive [7, 8]. The problem was that Michelson had used Newtonian physics, *viz* GaR, in calibrating the interferometer. Michelson and Morley detected fringe shifts, but they were smaller than expected, and were interpreted as a null effect: there was no aether or PFR effect. However Lorentz [30, 31] and Fitzgerald [32] offered an alternative explanation: physical objects, such as the arms supporting the interferometer optical elements, undergo a contraction in the direction of movement through the aether, or more generally relative to the PFR: the length becoming $L = L_0 \sqrt{1 - v_R^2/c^2}$, where $L_0$ is the physical length when at rest wrt the PFR, and $v_R$ is the speed relative to the PFR. It must be noted that this is not the Lorentz contraction effect predicted by SR, as discussed later, as that involves $L = L_0 \sqrt{1 - v_O^2/c^2}$, where $v_O$ is the speed of the arm or *any* space interval relative to the observer. The difference between these two predictions is stark, and has been observed experimentally, and the SR prediction is proven wrong.

Next consider two observers, $O$ and $O'$, in relative motion. Then the actual intrinsic or physical time and space coordinates of each are, in both LR and nLR, related by the Galilean transformation, and here we consider only a uniform $\mathbf{v}$: these coordinates are not the directly measured distances/time intervals - they require corrections to give the intrinsic values. We have taken the simplest case where $V$ is the intrinsic relative speed of the two observers in their common $x$ directions. Then from (1) the derivatives are related by

$$\frac{\partial}{\partial t} = \frac{\partial}{\partial t'} - V\frac{\partial}{\partial x'}, \frac{\partial}{\partial x} = \frac{\partial}{\partial x'}, \frac{\partial}{\partial y} = \frac{\partial}{\partial y'}, \frac{\partial}{\partial z} = \frac{\partial}{\partial z'}.$$

In the general case space rotations may be made.Then (3) becomes for the 2nd observer, with $v' = v - V$,

$$\left(\frac{\partial}{\partial t'} + \mathbf{v}' \cdot \nabla'\right)^2 \mathbf{A}'(\mathbf{r}', t') = c^2 \nabla'^2 \mathbf{A}'(\mathbf{r}', t'). \qquad (4)$$

with $\mathbf{A}'(\mathbf{r}', t') = \mathbf{A}(\mathbf{r}, t)$. If the flow velocity $\mathbf{v}(\mathbf{r}, t)$ is not uniform then we obtain refraction effects for the EM waves, capable of producing gravitational lensing. Only for an observer at rest in a time independent and uniform aether (LR) or dynamical space (nLR) does $v'$ disappear from (4).

# 5 Special Relativity from Galilean Relativity

The above uses physically intrinsic choices for the time and space coordinates, which are experimentally accessible. However we could choose to use a new class of time and space coordinates, indicated by upper-case symbols $T, X, Y, Z$, that mixes the above time and space coordinates. We begin by showing that Special Relativity (SR), with its putative spacetime as the foundation of reality, is nothing more than Galilean Relativity (GaR) written in terms of these mixed space and time coordinates. The failure to discover this, until 2008 [13] reveals one of the most fundamental blunders in

*The now standard formalism was actually done by Heaviside.

physics. One class of such mixed coordinates for $O$ is*

$$\begin{aligned} T &= \gamma(v)\left((1-\frac{v^2}{c^2})t+\frac{vx}{c^2}\right), \\ X &= \gamma(v)x,\ Y=y,\ Z=z \end{aligned} \tag{5}$$

where $v$ is the uniform speed of space (in the $x$ direction), and where $\gamma(v)=1/\sqrt{1-v^2/c^2}$. Note that this is not a Lorentz transformation. If an object has speed $w$, $x=wt$, wrt to $O$, then it has speed $W$, $X=WT$, using the mixed coordinates, wrt $O$

$$W=\frac{w}{1-\frac{v^2}{c^2}+\frac{v}{c^2}w} \tag{6}$$

Similarly for $O'$ using $v'$, $w'$ and $W'$. In particular (6) gives for the relative speed of $O'$ wrt $O$ in the mixed coordinates

$$\overline{V}=\frac{V}{1-\frac{v^2}{c^2}+\frac{v}{c^2}V} \tag{7}$$

Using the above we may now express the Galilean speed transformation (2) in terms of $W', W$ and $\overline{V}$ for the mixed coordinates, giving

$$W'=\frac{W-\overline{V}}{1-W\overline{V}/c^2} \tag{8}$$

which is the usual SR transformation for speeds, but here derived exactly from the Galilean transformation. Note that $c$ enters here purely because of the definitions in (5), which is designed to ensure that wrt the mixed space-time coordinates the speed of light is invariant: $c$. To see this note that from (5) the transformations for the derivatives are found to be

$$\begin{aligned} \frac{\partial}{\partial t} &= \gamma(v)\left(1-\frac{v^2}{c^2}\right)\frac{\partial}{\partial T}, \\ \frac{\partial}{\partial x} &= \gamma(v)\left(\frac{v}{c^2}\frac{\partial}{\partial T}+\frac{\partial}{\partial X}\right), \\ \frac{\partial}{\partial y} &= \frac{\partial}{\partial Y},\ \frac{\partial}{\partial z}=\frac{\partial}{\partial Z}. \end{aligned} \tag{9}$$

$\overline{\nabla}=\{\frac{\partial}{\partial X},\frac{\partial}{\partial Y},\frac{\partial}{\partial Z}\}$. Then we have from (3), for uniform $v$,

$$\left(\frac{\partial}{\partial T}\right)^2\overline{\mathbf{A}}(\mathbf{R},T)=c^2\overline{\nabla}^2\overline{\mathbf{A}}(\mathbf{R},T).$$

with $\mathbf{R}=\{X,Y,Z\}$ and $\overline{\mathbf{A}}(\mathbf{R},T)=\mathbf{A}(\mathbf{r},t)$. The speed of EM waves is now $c$ for all observers. This is a remarkable result. In the new class of coordinates the dynamical equation no longer contains the space velocity $\mathbf{v}$ - it has been mapped out of the dynamics. The EM dynamics is now invariant under Lorentz transformations.

$$\begin{aligned} T' &= \gamma(\overline{V})\left(T-\frac{\overline{V}X}{c^2}\right), \\ X' &= \gamma(\overline{V})(X-\overline{V}T),\ Y'=Y,\quad Z'=Z, \end{aligned} \tag{10}$$

*It is important to use different notation for the GaR coordinates and the SR coordinates: often the same notation is used, illustrating the confusion in this subject.

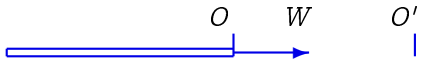


Figure 1: Here is derivation of SR length contraction from Galilean Relativity using coordinates introduced in (5). Consider two events: (1) RH end of rod travelling with observer $O$, with speed $W$ wrt observer $O'$, passes $O'$, and (2) when LH end passes $O'$. Then $dX'=0$, and $L'=WdT'$ defines $L'$. For $O$ $dX=L$ and $L=WdT$. Then (11) gives $L'=\sqrt{1-W^2/c^2}L$, with $W$ the speed of the rod wrt $O'$. However this is purely a coordinate effect, and has no physical significance. Experiment shows that it is the speed of the rod wrt space, $v_R$, that actually determines the length contraction.

and we note that for two events with coordinate differences $\{dT,dX\}$ or $\{dT',dX'\}$

$$dI^2\equiv c^2dT'^2-dX'^2=c^2dT^2-dX^2 \tag{11}$$

defines the invariant interval for different observers.

There is now no reference to the underlying flowing space: for an observer using this class of space and time coordinates the speed of EM waves relative to the observer is always $c$ and so invariant - there will be no EM speed anisotropy. We could also introduce, following Minkowski, "spacetime" light cones along which $d\tau^2=dT^2-d\mathbf{R}^2/c^2=0$. Note that $d\tau^2$ is invariant under the Lorentz transformation (10). Then pairs of spacetime events could be classified into either time-like, $d\tau^2>0$, or space-like, $d\tau^2\leq 0$, with the time ordering of spacelike events not being uniquely defined. However this outcome is merely an artefact of the mixed space-time coordinates: $dT$ is not the actual time interval.

Confusing a space and time coordinate system with actual space and time phenomena has confounded physics for more than 100 years, with this illustrated above by the recently discovered exact relationship between Galilean Relativity and Einstein Relativity. In mainstream physics it is claimed that Special Relativity reduces to Galilean Relativity only in the limit of speeds small compared to $c$. But the various so-called "relativistic effects" ascribed to Special Relativity are nothing more than coordinate effects - they are not real. It was Lorentz who first gave a possible *dynamical* account of relativistic effects, namely that they are caused by absolute motion of objects relative to the aether (LR) or, now, dynamical space (nLR), which according to the evidence discussed above, is absolute motion relative to a dynamical and structured quantum foam substratum: space. In Lorentz Relativity relativistic effects are genuine dynamical effects and must be derived from some dynamical theory. This has yet to be done, and for the length contraction effect would involve the quantum theory of matter.

Finally we note in Fig.1 that the so-called length contraction effect in SR is exactly derivable from GaR - and so it is purely a coordinate effect, and so has no physical meaning.

We note that the Lorentz transformation (10) is not relevant to nLR.

# 6 Detecting Lorentz Relativistic Effects

We now show how only Lorentz Relativity gives a valid account of the experimental results dealing with light speed anisotropy. To that end we consider the differing predictions made by the relativity theories for the length contraction effect, and we use data from Michelson interferometer experiments, which being a 2nd order in $v/c$ detector requires length contraction effects to be included, when relevant. These contradictory predictions are compared with detailed data from the NASA spacecraft earth-fly Doppler shifts, which in LR and nLR do not involve any length contraction, as no objects/supporting arms are involved. The flyby Doppler shifts have been also confirmed by laboratory 1st order $v/c$ experiments by DeWitte and Cahill, see [20], and so not requiring 2nd order $v/c$ length contraction effects to be considered. So we have a critical and decisive test of the relativity theories. In all cases we parametrise the calibration theory for the Michelson interferometer travel time difference between the two arms according to

$$\Delta t = k^2 \frac{L_0 v_p^2}{c^3} \cos(2\theta) \tag{12}$$

where $k^2$ is the theory-dependent calibration constant. Here $L_0$ is the at-rest arm length, $v_P$ is the relevant velocity projected onto the plane of the interferometer, and $\theta$ is the angle between that projected velocity and one of the arms, see Fig.2.

Lorentz and neo-Lorentz Relativity Interferometer Calibration: In both LR and nLR the length contraction effect is a real dynamical effect caused by the absolute motion of an actual object wrt aether (LR) or dynamical space (nLR). A simple analysis yields the calibration constant $k^2 = (n^2 - 1)$, when $n \approx 1$ is the refractive index of the gas present: for air $n = 1.00029$ at STP, giving $k^2 = 0.00058$. Some data from the Michelson-Morley and Miller experiments are shown in Fig.3, showing, together with other data, that this value of $k^2$ gives excellent agreement with the Doppler shift data, and different 1st order in $v/c$ experiments [20]. The gas-mode interferometer experiments and spacecraft Doppler shift data give $v \approx 500$km/s. Note that high-accuracy vacuum-mode Michelson interferometers will give a null result ($n = 1$), as has been repeatedly observed.

Galilean Relativity Interferometer Calibration: In Galilean Relativity there is no length contraction effect, and repeating the analysis, without that effect, we obtain $k^2 = n^3$ ($\approx 1$ for air). This is the calibration constant used by Michelson-Morley in 1887. Using this to analyse their data they found that $v_P \leq 10$km/s. This is in stark conflict with the speed of $v \approx 500$km/s from spacecraft earth-flyby Doppler shift and 1st order in $v/c$ experiments. So Galilean Relativity is ruled out.

Einstein Relativity Interferometer Calibration: There are two routes to $k^2$ from Einstein Relativity, depending on which choice of space and time variables is used. Here we use the Galilean space and time coordinates, as we have shown that they are the physical coordinates that underly SR, in which case $k^2 = n^3$, giving $v_P \leq 10$km/s and so again is in stark disagreement with experimental data.

In a different approach we use the mixed space and time coordinates conventionally used in SR calculations. Then the speed of light is $c/n$ - invariant wrt to these coordinates, but there is no length contraction effect, because the arms are at rest wrt the observer. Then again we find that $k^2 = n^3 \approx 1$, and in disagreement with the experimental data.

# 7 Michelson Interferometer Detectors

The Michelson interferometer was a brilliantly conceived instrument for measuring light speed anisotropy. However Michelson made two critically incorrect assumptions, which inadvertently had the effect of misguiding physics for another 100 years and more. The 1st was to assume Newtonian physics in determining the calibration theory for the instrument, and the 2nd was to average data from successive days at the same approximate times, with the assumption being that this would average out "instrumental fluctuations", when it had the opposite effect because there were significant "gravitational wave" effects in the data, and these were different on different days, even at the same time.

We now have a clear understanding of the design principles of the Michelson interferometer as a detector of light speed anisotropy, and *ipso facto* as a detector for the actual 3-space flow turbulence/ gravitational waves, (Cahill and Kitto, [5]), (Cahill, [6, 7]). This is because two different and independent effects exactly cancel in vacuum mode. The key insight is that the dynamical space is describable at a macroscopic/classical level by a detectable velocity field $\mathbf{v}(\mathbf{r}, t)$, relative to an observer using spatial coordinate $\mathbf{r}$ and time coordinate $t$, both of which must be carefully determined so as to remove absolute motion effects, that is, effects caused by the motion of rods and clocks wrt space. The key aspects of the interferometer are shown in Fig.1. Taking account of the geometrical path differences, the Fitzgerald-Lorentz arm-length contraction and the Fresnel drag effect leads to the travel time difference between the two arms, and which is detected by interference effects*, is given by

*The dielectric of course does not cause the observed effect, it is merely a necessary part of the instrument design physics, just as mercury in a thermometer does not *cause* temperature.

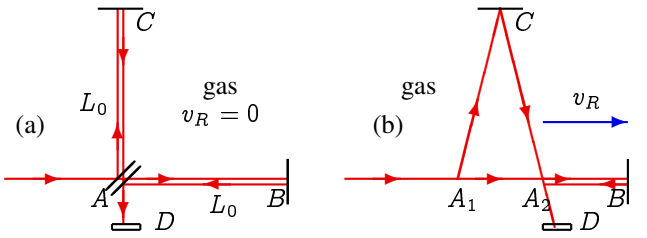


Figure 2: Schematic diagrams of the gas-mode Michelson Interferometer, with beam splitter/mirror at $A$ and mirrors at $B$ and $C$ mounted on arms from $A$, with the arms of equal length $L_0$ when at rest. $D$ is the detector screen. In (a) the interferometer is at rest in space. In (b) the instrument and gas are moving through 3-space with speed $v_R$ parallel to the $AB$ arm. Interference fringes are observed at $D$ when mirrors $B$ and $C$ are not exactly perpendicular - the Hick's effect. As the interferometer is rotated in the plane shifts of these fringes are seen in the case of absolute motion, but only if the apparatus operates in a gas. By measuring fringe shifts the speed $v_R$ may be determined.

$$\Delta t = k^2 \frac{L v_P^2}{c^3} \cos\big(2(\theta - \psi)\big), \tag{13}$$

where $\psi$ specifies the direction of $\mathbf{v}(\mathbf{r}, t)$ projected onto the plane of the interferometer, giving projected speed $v_P$, relative to the local meridian, and where $k^2 = (n^2 - 2)(n^2 - 1)$, with $n$ the refractive index. Neglect of the absolute motion relativistic Fitzgerald-Lorentz contraction effect gives $k^2 \approx n^3 \approx 1$ for gases, which is essentially the Newtonian theory that Michelson used.

We derive the calibration constant $k^2$ for the Michelson interferometers in the case of Lorentzian Relativity. The two arms are constructed to have the same lengths when they are physically parallel to each other. For convenience assume that the value $L_0$ of this length refers to the lengths when at rest wrt space The Fitzgerald-Lorentz effect is that the arm $AB$ parallel to the direction of motion is shortened to

$$L_{\|} = L_0 \sqrt{1 - \frac{v_R^2}{c^2}} \tag{14}$$

where $v_R$ is the lengthwise speed of the arm relative to space. In SR $v_R$ is the speed relative to the observer, who is presumably at rest wrt the arms, then $v_R = 0$ and there is no arm contraction effect.

For later reference we also give the time dilation expression for physical clocks:

$$\tau = T \sqrt{1 - \frac{v_R^2}{c^2}} \tag{15}$$

where $\tau$ is the elapsed time given by the clock, for an actual time interval $T$.

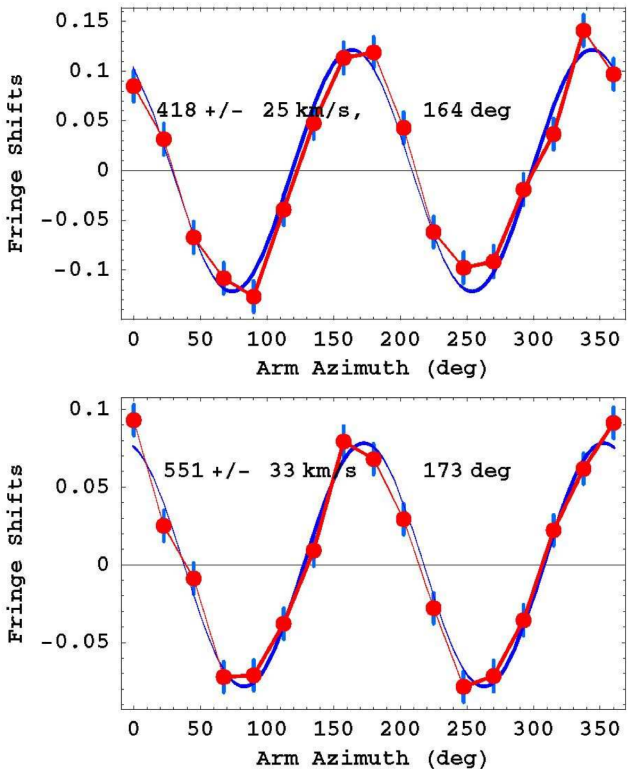


Figure 3: Top: Typical Miller data from 1925/26 gas-mode Michelson interferometer, from averaging 20 360° rotations, (Miller, 1933). Bottom: Data from Michelson-Morley 1887 gas-mode interferometer, from averaging 6 360° rotations. In both plots the non-orthogonal term and temperature drift effects have been removed from the data, after a least squares best fit using the full detector theory derived in the text, (22), (Michelson and Morley, 1887). This reduced data then shows an impressive agreement with the $\cos\big(2(\theta - \psi)\big)$ form.

For simplicity here we take the motion of the detector to be parallel to the arm AB. Following Fig.2 let the time taken for light to travel from $A \to B$ be $t_{AB}$ and that from $B \to A$ be $t_{BA}$, where $V$ is the speed of light relative to the gas, which is moving with the detector. We shall also neglect the Fresnel drag effect, so $V = c/n$. Then

$$V t_{AB} = L_{\|} + v_R t_{AB} \quad \text{and} \quad V t_{BA} = L_{\|} - v_R t_{BA}.$$

$$\begin{aligned} t_{ABA} = t_{AB} + t_{BA} &= \frac{L_{\|}}{V - v_R} + \frac{L_{\|}}{V + v_R} \\ &= \frac{2 L_0 V \sqrt{1 - \frac{v_R^2}{c^2}}}{V^2 - v_R^2}. \end{aligned} \tag{16}$$

For the other arm, with no contraction in its length,

$$(V t_{AC})^2 = L_0^2 + (v_R t_{AC})^2$$

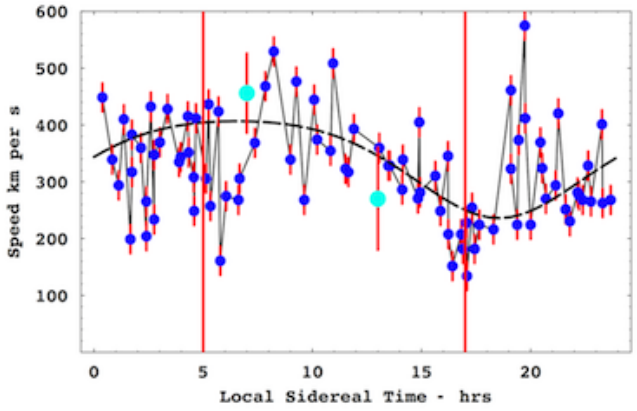


Figure 4: Speeds $v_P$, of the 3-space velocity $\mathbf{v}$ projected onto the horizontal plane of the Miller gas-mode Michelson interferometer located atop Mt.Wilson, plotted against local sidereal time in hours, for a composite day, with data collected over a number of days in September 1925. The data shows considerable fluctuations, from hour to hour, and also day to day, as this is a composite day. The dashed curve shows the non-fluctuating best-fit variation over one day, as the earth rotates, causing the projection onto the plane of the interferometer of the velocity of the average direction of the space flow to change. The maximum projected speed of the curve is 417 km/s (using the STP air refractive index of $n = 1.00029$, and the min/max occur at approximately 5hrs and 17hrs local sidereal time (Right Ascension). Note that the Cassini flyby in August, [16], gives a RA= $5.15^h$, close to the RA apparent in the above plot. The data points, with error bars, at $7^h$ and $13^h$ are from the Michelson-Morley 1887 data, from averaging (excluding only the July 8 data for $7^h$ because it has poor S/N). The fiducial time lines are at $5^h$ and $17^h$. The speed fluctuations are seen to be much larger than the statistically determined errors, confirming the presence of turbulence in the 3-space flow, i.e gravitational waves, as first seen in the Michelson-Morley experiment.

$$t_{AC} = \frac{L_0}{\sqrt{V^2 - v_R^2}}, \quad t_{ACA} = 2t_{AC} = \frac{2L_0}{\sqrt{V^2 - v_R^2}}, \tag{17}$$

giving finally for the travel time difference for the two arms

$$\Delta t = \frac{2L_0 V\sqrt{1 - \frac{v_R^2}{c^2}}}{V^2 - v_R^2} - \frac{2L_0}{\sqrt{V^2 - v_R^2}}. \tag{18}$$

Now trivially $\Delta t = 0$ if $v_R = 0$, but also $\Delta t = 0$ when $v_R \neq 0$ but only if $V = c$, *viz* vacuum. This then would result in a null result on rotating the apparatus. Hence the null result of the Michelson apparatus is only for the special case of light travelling in vacuum. However if the apparatus is immersed in a gas then $V < c$ and a non-null effect is expected on rotating the apparatus, since now $\Delta t \neq 0$. It is essential then in analysing data to correct for this refractive index effect. Putting $V = c/n$ in (18) we find, for $v_R \ll V$ and when $n \approx 1$, that

$$\Delta t = n(n^2 - 1)\frac{L_0 v_R^2}{c^3}. \tag{19}$$

However if the data is analysed not using the Fitzgerald-Lorentz contraction (14), then, as done in the old analyses, the estimated time difference is

$$\Delta t = \frac{2L_0 V}{V^2 - v_R^2} - \frac{2L_0}{\sqrt{V^2 - v_R^2}}, \tag{20}$$

which again for $v_R \ll V$ gives

$$\Delta t = n^3\frac{L_0 v_R^2}{c^3}. \tag{21}$$

With Fresnel drag and $n \approx 1$, the sign of $\Delta t$ is reversed. Symmetry arguments easily show that when rotated we obtain a $\cos(2\theta)$ factor.

However the above analysis does not correspond to how the interferometer is actually operated. That analysis does not actually predict fringe shifts, for the field of view would be uniformly illuminated, and the observed effect would be a changing level of luminosity rather than fringe shifts. As Michelson and Miller knew, the mirrors must be made slightly non-orthogonal with the degree of non-orthogonality determining how many fringe shifts were visible in the field of view. Experimenting with this effect determines a comfortable number of fringes: not too few and not too many. The non-orthogonality reduces the symmetry of the device, and instead of having period of 180° the symmetry now has a period of 360°, so that we must add the extra term $a\cos(\theta - \beta)$ in

$$\Delta t = k^2\frac{L(1 + e\theta)v_P^2}{c^3}\cos\big(2(\theta - \psi)\big) + a(1 + e\theta)\cos(\theta - \beta) + f \tag{22}$$

The factor $1 + e\theta$ models the temperature effects, namely that as the arms are uniformly rotated, one rotation taking several minutes, there will also be a temperature induced change in the length of the arms. If the temperature effects are linear in time, as they would be for short time intervals, then they are linear in $\theta$. In the non-orthogonality term the parameter $a$ is proportional to the length of the arms, and so also has the temperature factor. The term $f$ simply models any offset effect. Michelson and Morley and Miller took these two effects into account when analysing his data.

The interferometers are operated with the arms horizontal. Then $\theta$ is the azimuth of one arm relative to the local meridian, while $\psi$ is the azimuth of the absolute motion velocity projected onto the plane of the interferometer, with projected component $v_P$. Here the Fitzgerald-Lorentz contraction is a real dynamical effect of absolute motion, unlike the Einstein spacetime view that it is merely a spacetime perspective artifact, and whose magnitude depends on

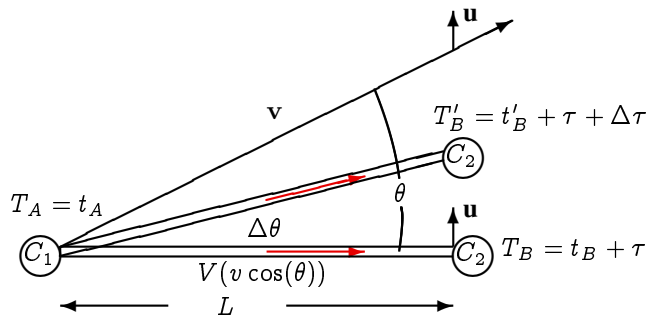


Figure 5: Schematic layout for measuring the one-way speed of light in either free-space, optical fibers or RF coaxial cables, without requiring the synchronisation of the clocks $C_1$ and $C_2$. Here $\tau$ is the, initially unknown, offset time between the clocks. Times $t_A$ and $t_B$ are true times, without clock offset and clock transport effects, while $T_A = t_A$, $T_B = t_A + \tau$ and $T'_B = t'_B + \tau + \Delta\tau$ are clock readings. $V(v\cos(\theta))$ is the speed of EM radiation wrt the apparatus before rotation, and $V(v\cos(\theta - \Delta\theta))$ after rotation, $\mathbf{v}$ is the velocity of the apparatus through space in direction $\theta$ relative to the apparatus before rotation, $\mathbf{u}$ is the velocity of transport for clock $C_2$, and $\Delta\tau < 0$ is the net slowing of clock $C_2$ from clock transport, when apparatus is rotated through angle $\Delta\theta > 0$. Note that $\mathbf{v}\cdot\mathbf{u} > 0$.

the choice of observer. The instrument is operated by rotating at a rate of one rotation over several minutes, and observing the shift in the fringe pattern through a telescope during the rotation. Then fringe shifts from six (Michelson and Morley) or twenty (Miller) successive rotations are averaged to improve the signal to noise ratio, and the average sidereal time noted. Some examples are shown in Fig.2, and illustrate the incredibly clear signal. The ongoing claim that the Michelson-Morley experiment was a null experiment is disproved. Fig.4 shows data from these two experiments over a 24hr sidereal day. The large fluctuations are gravitational wave effects, and have been seen in all experiments that detected light speed anisotropy.

# 8 DeWitte RF Coaxial Cable Detector

The enormously significant 1991 DeWitte double one-way 1st order in $v/c$ experiment successfully measured the anisotropy of the speed of RF EM waves using clocks at each end of the RF coaxial cables [12, 21]. The technique uses rotation of the coaxial cables, by means of the earth rotation, to permit extraction of the EM speed anisotropy, despite the clocks not being synchronised. Data from this 1st order in $v/c$ experiment agrees with the speed and direction of the anisotropy results from all the other experiments reported herein.

Fig.5 shows the arrangement for measuring the one-way speed of light, either in vacuum, a dielectric, or RF coaxial cable. It is usually argued that one-way speed of light measure-

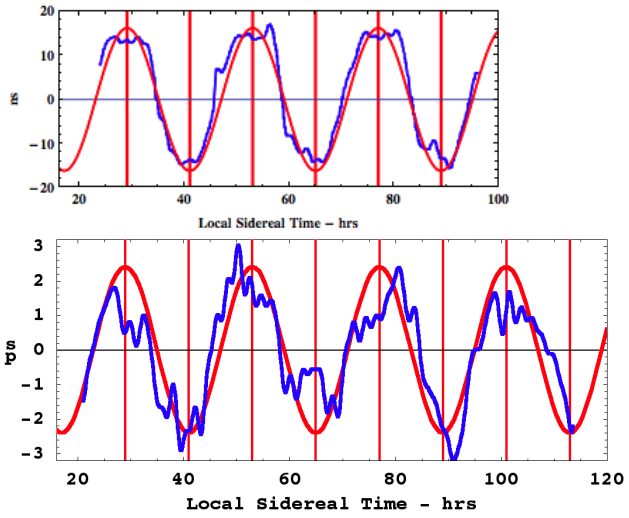


Figure 6: Top: Data from the 1991 DeWitte NS RF coaxial cable experiment, $L = 1.5$km, using the arrangement shown in Fig.5, with a 2nd RF coaxial cable carrying a signal in the reverse direction. The vertical red lines are at RA=$5^h$. DeWitte gathered data for 178 days, and showed that the crossing time tracked sidereal time, and not local solar time, see Fig.7. DeWitte reported that $v \approx 500km/s$. If the full Fresnel drag effect is included no effect would have been seen. Bottom: Dual RF coaxial cable detector data from May 2009, Cahill [16], using the technique in Fig.12 with $L = 20$m. NASA Spacecraft Doppler shift data predicts Dec$= -77^\circ$, $v = 480$km/s, giving a sidereal dynamic range of 5.06ps, very close to that observed. The vertical red lines are at RA=$5^h$. In both data sets we see the earth sidereal rotation effect together with significant wave/turbulence effects.

ments are not possible because the clocks $C_1$ and $C_2$ cannot be synchronised. However this is false. An important effect that needs to be included is the clock offset effect caused by transport, when the apparatus is rotated in this case, but most significantly the Fresnel drag effect is not present in RF coaxial cables, at low RF frequencies. In Fig.5 the actual travel time $t_{AB} = t_B - t_A$ from $A$ to $B$, as distinct from the clock indicated travel time $T_{AB} = T_B - T_A$, is determined by

$$V(v\cos(\theta))t_{AB} = L + v\cos(\theta)t_{AB} \tag{23}$$

where the 2nd term comes from the end $B$ moving an additional distance $v\cos(\theta)t_{AB}$ during time interval $t_{AB}$. With Fresnel drag $V(v) = \frac{c}{n} + v\left(1 - \frac{1}{n^2}\right)$, when $V$ and $v$ are parallel, and where $n$ is the dielectric refractive index. Then

$$t_{AB} = \frac{L}{V(v\cos(\theta)) - v\cos(\theta)} = \frac{nL}{c} + \frac{v\cos(\theta)L}{c^2} + .. \tag{24}$$

However if there is no Fresnel drag effect, $V = c/n$, as is the case in RF coaxial cables, then we obtain

$$t_{AB} = \frac{L}{V(v\cos(\theta)) - v\cos(\theta)} = \frac{nL}{c} + \frac{v\cos(\theta)Ln^2}{c^2} + .. \tag{25}$$

It would appear that the two terms in (24) or (25) can be separated by rotating the apparatus, giving the magnitude and direction of $\mathbf{v}$. However it is $T_{AB} = T_B - T_A$ that is measured, and not $t_{AB}$, because of an unknown fixed clock offset $\tau$, as the clocks are not *a priori* synchronised, and as well an angle dependent clock transport offset $\Delta\tau$, at least until we can establish clock synchronisation, as explained below. Then the clock readings are $T_A = t_A$ and $T_B = t_B + \tau$, and $T'_B = t'_B + \tau + \Delta\tau$, where $\Delta\tau$ is a clock offset that arises from slowing of clock $C_2$ as it is transported during the rotation through angle $\Delta\theta$, see Fig.5.

The clock transport offset $\Delta\tau$ follows from the clock motion effect [21]

$$\Delta\tau = dt\sqrt{1-\frac{(\mathbf{v}+\mathbf{u})^2}{c^2}} - dt\sqrt{1-\frac{\mathbf{v}^2}{c^2}} = -dt\frac{\mathbf{v}\cdot\mathbf{u}}{c^2} + \ldots, \tag{26}$$

when clock $C_2$ is transported at velocity $\mathbf{u}$ over time interval $dt$, compared to $C_1$. Now $\mathbf{v}\cdot\mathbf{u} = vu\sin(\theta)$ and $dt = L\Delta\theta/u$. Then the change in $T_{AB}$ from this small rotation is, using (25) for the case of no Fresnel drag,

$$\Delta T_{AB} = -\frac{v\sin(\theta)Ln^2\Delta\theta}{c^2} + \frac{v\sin(\theta)L\Delta\theta}{c^2} + \ldots \tag{27}$$

as the clock transport effect appears to make the clock-determined travel time longer (2nd term). Integrating we get

$$T_B - T_A = \frac{nL}{c} + \frac{v\cos(\theta)L(n^2-1)}{c^2} + \tau, \tag{28}$$

where $\tau$ is now the constant offset time. The $v\cos(\theta)$ term may be separated by means of the angle dependence. Then the value of $\tau$ may be determined, and the clocks synchronised. However if the propagation medium is liquid, or dielectrics such as glass and optical fibers, the Fresnel drag effect is present, and we then use (24), and not (25). Then in (28) we need make the replacement $n \to 1$, and then the 1st order in $v/c$ term vanishes. However, in principle, separated clocks may be synchronised by using RF coaxial cables.

The DeWitte $L = 1.5$km 5MHz RF coaxial cable experiment, in Brussels in 1991, was a double 1st order in $v/c$ detector, using the scheme in Fig.5, but employing a 2nd RF coaxial cable for the opposite direction, giving clock difference $T_C - T_D$, to cancel temperature effects, and also used 3 Caesium atomic clocks at each end. The orientation was NS and rotation was achieved by that of the earth. Then

$$T_{AB} - T_{CD} = \frac{2v\cos(\theta)L(n^2-1)}{c^2} + 2\tau \tag{29}$$

For a horizontal detector the dynamic range of $\cos(\theta)$ is $2\sin(\lambda)\cos(\delta)$, caused by the earth rotation, where $\lambda$ is the latitude of the detector location and $\delta$ is the declination of $\mathbf{v}$. The value of $\tau$ may be determined and the clocks synchronised. Some of DeWiite's data and results are in Figs.6 and 7.

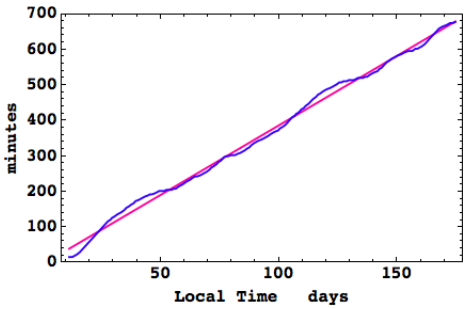


Figure 7: DeWitte collected data over 178 days and demonstrated that the zero crossing time, see Fig.6, tracked sidereal time and not local solar time. The plot shows the negative of the drift in the crossing time vs local solar time, and has a slope, determined by the best-fit straight line, of -3.918 minutes per day, compared to the actual average value of -3.932 minutes per day, the difference between a sidereal day and a solar day.

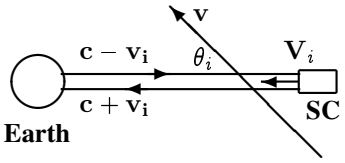


Figure 8: Asymptotic flyby configuration in earth frame-of-reference, with spacecraft (SC) approaching Earth with velocity $\mathbf{V}_i$. The departing asymptotic velocity will have a different direction but the same speed, as no force other than conventional Newtonian gravity is assumed to be acting upon the SC. The dynamical 3-space velocity is $\mathbf{v}(\mathbf{r},t)$, though taken to be time independent during the Doppler shift measurement, which causes the outward EM beam to have speed $c - v_i(r)$, and inward speed $c + v_i(r)$, where $v_i(r) = v(r)\cos(\theta_i)$, with $\theta_i$ the angle between $\mathbf{v}$ and $\mathbf{V}$. A similar description applies to the departing SC, labeled $i \to f$.

We see that DeWitte's RF EM speed anisotropy experiment is consistent with other experiments, and also shows significant fluctuations.

# 9 Earth Flyby RF Doppler Shifts: 3-Space Flow

The motion of spacecraft relative to the earth are measured by observing the direction and Doppler shift of the transponded RF EM transmissions. This gives another technique to determine the speed and direction of the dynamical 3-space as manifested by the light speed anisotropy [16] The repeated detection of the anisotropy of the speed of light has been, until recently, ignored in analysing the Doppler shift data, causing the long-standing anomalies in the analysis [1]. The use of the Minkowski-Einstein choice of time and space coordinates does not permit the analysis of these Doppler anomalies, as they mandate that the speed of the EM waves be invariant.

Because we shall be extracting the earth inflow effect we

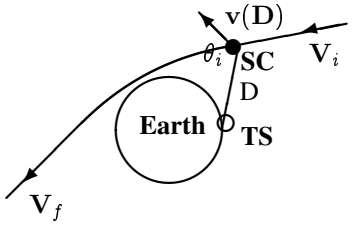


Figure 9: Spacecraft (SC) earth flyby trajectory, with initial and final asymptotic velocity $\mathbf{V}$, differing only by direction. The Doppler shift is determined from Fig.8 and (43). The 3-space flow velocity at the location of the SC is $\mathbf{v}$. The line joining Tracking Station (TS) to $SC$ is the path of the RF signals, with length $D$. As SC approaches earth $\mathbf{v}(D)$ changes direction and magnitude, and hence magnitude of projection $v_i(D)$ also changes, due to earth component of 3-space flow and also because of RF direction to/from Tracking Station. The SC trajectory averaged magnitude of this earth in-flow is determined from the flyby data and compared with theoretical prediction.

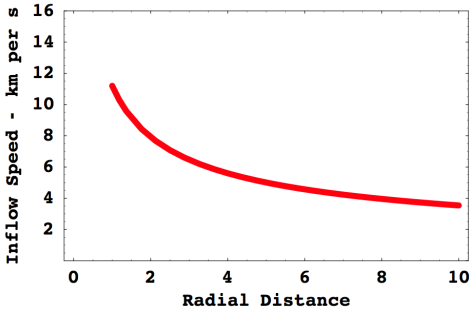


Figure 10: Predicted Earth 3-space inflow speed vs distance from earth in earth radii $v = \sqrt{2GM/R}$, plotted only for $R > 1.0$. Combining the NASA/JPL optical fiber RA determination and the flyby Doppler shift data has permitted the determination of the angle- and distance-averaged inflow speed, to be $12.4 \pm 5$km/s.

need to take account of a spatially varying, but not time-varying, 3-space velocity. In the earth frame of reference, see Fig.8, and using clock times from earth-based clocks, let the transmitted signal from earth have frequency $f$. The time for one RF maximum to travel distance $D$ to SC from earth is, see Fig.9,

$$t_1 = \int_0^D \frac{dr}{c - v_i(r)} \tag{30}$$

The next RF maximum leaves time $T = 1/f$ later and arrives at SC at time, taking account of SC motion,

$$t_2 = T + \int_0^{D-VT} \frac{dr}{c - v_i(r)} \tag{31}$$

The period at the SC of the arriving RF is then

$$T' = t_2 - t_1 = T + \int_D^{D-VT} \frac{dr}{c - v_i(r)} \approx \frac{c - v_i(D) - V}{c - v_i(D)} T \tag{32}$$

Essentially this RF is reflected* by the SC. Then the 1st RF maximum takes time to reach the earth

$$t_1' = -\int_D^0 \frac{dr}{c + v_i(r)} \tag{33}$$

and the 2nd RF maximum arrives at the later time

$$t_2' = T' - \int_{D-VT'}^0 \frac{dr}{c + v_i(r)}. \tag{34}$$

Then the period of the returning RF at the earth is

$$T'' = t_2' - t_1' \tag{35}$$

$$= T' + \int_D^{D-VT'} \frac{dr}{c + v_i(r)} \tag{36}$$

$$\approx \frac{c + v_i(D) - V}{c + v_i(D)} T' \tag{37}$$

Then overall we obtain the return frequency to be

$$f'' = \frac{1}{T''} = \frac{c + v_i(D)}{c + v_i(D) - V} \cdot \frac{c - v_i(D)}{c - v_i(D) - V} f \tag{38}$$

Ignoring the projected 3-space velocity $v_i(D)$, that is, assuming that the speed of light is invariant as per the usual literal interpretation of the Einstein 1905 light speed postulate, we obtain instead

$$f'' = \frac{c^2}{(c - V)^2} f. \tag{39}$$

The use of (39) instead of (38) is the origin of the putative anomalies. Expanding (39) we obtain

$$\frac{\Delta f}{f} = \frac{f'' - f}{f} = \frac{2V}{c} \tag{40}$$

However expanding (38) we obtain, for the same Doppler shift,

$$\frac{\Delta f}{f} = \frac{f'' - f}{f} = \left(1 + \frac{v(D)^2}{c^2}\right) \frac{2V}{c} + .... \tag{41}$$

It is the prefactor to $2V/c$ missing from (40) that explains the spacecraft Doppler anomalies, and also permits yet another determination of the 3-space velocity $\mathbf{v}(D)$ at the location of the SC. The published data does not give the Doppler shifts as a function of SC location, so the best we can do at present is to use a SC trajectory-averaged $v(D)$, namely $\overline{v}_i$ and $\overline{v}_f$, for the incoming and outgoing trajectories, as further discussed below.

From the observed Doppler shift data acquired during a flyby, and then best fitting the trajectory, the asymptotic hyperbolic speeds $V_{i\infty}$ and $V_{f\infty}$ are inferred from (40), but incorrectly so, as in Anderson [1]. These inferred asymptotic speeds may be related to an inferred asymptotic Doppler shift

$$\frac{\Delta f_{i\infty}}{f} = \frac{f_\infty' - f}{f} = \frac{2V_{i\infty}}{c} + .. \tag{42}$$

*In practice a more complex protocol is used.

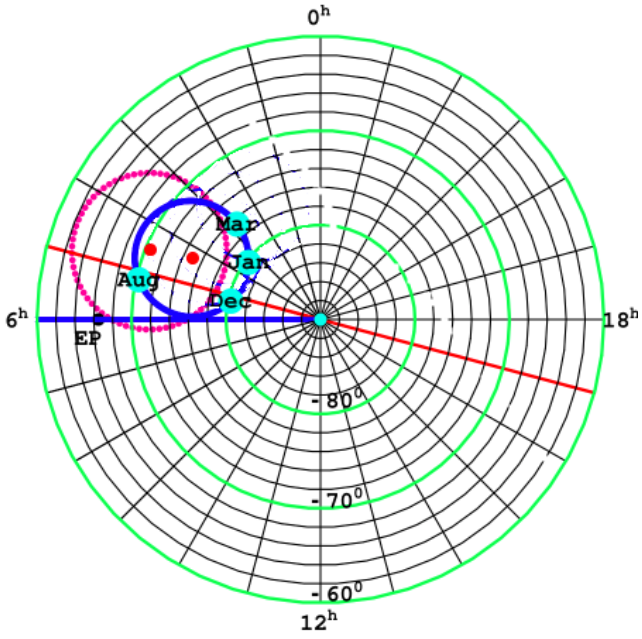


Figure 11: South celestial pole region. The dot at RA=4.3$^h$, Dec=75°S, and with speed 486km/s, is the direction of motion of the solar system through space determined from NASA spacecraft earth-flyby Doppler shifts, revealing the EM radiation speed anisotropy. The thick circle centred on this direction is the observed velocity direction for different days of the year, caused by earth orbital motion and sun 3-space inflow. The corresponding results from the Miller gas-mode interferometer are shown by 2nd dot and its aberration circle. For December 8, 1992, the velocity is RA=5.2$^h$, Dec=80°S, speed 491km/s.

which from (41) gives

$$V_{i\infty} \equiv \frac{\Delta f_{i\infty}}{f}.\frac{c}{2} = \left(1 + \frac{\overline{v}_i^2}{c^2}\right) V + .... \qquad (43)$$

where $V$ is the actual asymptotic speed. Similarly after the flyby we obtain

$$V_{f\infty} \equiv \frac{\Delta f_{f\infty}}{f}.\frac{c}{2} = \left(1 + \frac{\overline{v}_f^2}{c^2}\right) V + .... \qquad (44)$$

and we see that the "asymptotic" speeds $V_{i\infty}$ and $V_{f\infty}$ must differ, as indeed reported in Anderson, 2008 [1]. We then obtain the expression for the so-called flyby anomaly

$$\Delta V_\infty = V_{f\infty} - V_{i\infty} = \frac{\overline{v}_f^2 - \overline{v}_i^2}{c^2} \qquad (45)$$

where here $V \approx V_\infty$ to sufficient accuracy, where $V_\infty$ is the average of $V_{i\infty}$ and $V_{f\infty}$, The existing data on $\mathbf{v}$ permits *ab initio* predictions for $\Delta V_\infty$. As well a separate least-squares-fit to the individual flybys permits the determination of the average speed and direction of the 3-space velocity, relative to the earth, during each flyby. These results are all remarkably consistent with the data from the various laboratory experiments that studied $\mathbf{v}$. We now indicate how $\overline{v}_i$ and $\overline{v}_f$ were parametrised during the best-fit to the flyby data. $\mathbf{v}_{galactic} + \mathbf{v}_{sun} - \mathbf{v}_{orbital}$ is taken as constant during each individual flyby, with $\mathbf{v}_{sun}$ inward towards the sun, with value 42 km/s, and $\mathbf{v}_{orbital}$ as tangential to earth orbit with value 30 km/s - consequentially the directions of these two vectors changed with day of each flyby. This linear superposition is only approximate, Cahill [14]. The earth in-flow $\mathbf{v}_{earth}$ was taken as radial and of an unknown fixed trajectory-averaged value. So the averaged direction but not the averaged speed varied from flyby to flyby, with the incoming and final direction being approximated by the $(\alpha_i, \delta_i)$ and $(\alpha_f, \delta_f)$ asymptotic directions. The predicted theoretical variation of $v_{earth}(R)$ is shown in Fig.10. This results in the plot in Fig.11 and the earth in-flow speed determination. The results are in remarkable agreement with the results from Miller, showing the extraordinary skill displayed by Miller in carrying out his massive interferometer experiment and data analysis in 1925/26. The only effect missing from the Miller analysis is the spatial in-flow effect into the sun, which affected his data analysis. Miller obtained a galactic flow direction of $\alpha = 4.52$ hrs, $\delta = -70.5°$, compared to that obtained herein from the NASA data of $\alpha = 4.29$ hrs, $\delta = -75.0°$, which differ by only $\approx 5°$.

As well the flyby Doppler shifts show considerable fluctuations. We conjecture that these are gravitational wave effects, although no analysis has been done to characterise these fluctuations.

The numerous EM anisotropy experiments discussed herein demonstrate that a dynamical 3-space exists, and that the speed of the earth wrt this space exceeds 1 part in 1000 of $c$, namely a large effect. Not surprisingly this has indeed been detected many times over the last 127 years. The speed of ~500 km/s means that earth based clocks experience a real, so-called, time dilation effect from (15) of approximately 0.12s per day compared to cosmic time. However clocks may be corrected for this clock dilation effect because their speed $v$ though space, which causes their slowing, is measurable by various experimental methods. This means that the absolute or cosmic time of the universe is measurable. This very much changes our understanding of time. However because of the inhomogeneity of the earth 3-space in-flow component the clock slowing effect causes a differential effect for clocks at different heights above the earth's surface. It was this effect that Pound and Rebka reported in 1960 using the Harvard tower [35]. Consider two clocks at heights $h_1$ and $h_2$, with $h = h_2 - h_1$, then the frequency differential follows from

(15),

$$\frac{\Delta f}{f} = \sqrt{1-\frac{v^2(h_2)}{c^2}} - \sqrt{1-\frac{v^2(h_1)}{c^2}} \quad (46)$$

$$\approx \frac{v^2(h_1)-v^2(h_2)}{2c^2} + .. \quad (47)$$

$$= \frac{1}{2c^2}\frac{dv^2(r)}{dr}h + .. \quad (48)$$

$$= \frac{g(r)h}{c^2} + .. \quad (49)$$

$$= -\frac{\Delta\Phi}{c^2} + .. \quad (50)$$

where $\Phi$ is the so-called 'gravitiational potential', and with $\mathbf{v}.\nabla\mathbf{v} = \nabla\left(\frac{v^2}{2}\right)$ for zero vorticity $\nabla\times\mathbf{v} = \mathbf{0}$, and ignoring any time dependence of the flow, and where finally, $\Delta\Phi$ is the change in the gravitational potential. The actual process here is that, say, photons are emitted at the top of the tower with frequency $f$ and reach the bottom detector with the same frequency $f$ - there is no change in the frequency. This follows from (32) but with now $V = 0$ giving $T = T'$. However the bottom clock is running slower because the speed of space there is faster, and so this clock determines that the falling photon has a higher frequency, ie. appears blue shifted. The opposite effect is seen for upward travelling photons, namely an apparent red shift as observed by the top clock. In practice the Pound-Rebka experiment used motion induced Doppler shifts to make these measurements using the Mössbauer effect. The overall conclusion is that Pound and Rebka measured the derivative of $v^2$ wrt height, whereas herein we have measured that actual speed, but averaged wrt the SC trajectory measurement protocol. It is important to note that the so-called "time dilation" effect is really a "clock slowing" effect - clocks are simply slowed by their movement through 3-space. The Gravity Probe A experiment also studied the clock slowing effect, though again interpreted differently therein, and again complicated by additional Doppler effects.

The Cosmic Microwave Background (CMB) velocity is often confused with the Absolute Motion (AM) velocity or light-speed anisotropy velocity as determined in the experiments discussed herein. However these are unrelated and in fact point in very different directions, being almost at $90^0$ to each other, with the CMB velocity being 369 km/s in direction $(\alpha = 11.2^h, \delta = -7.22^0)$.

The CMB velocity is obtained by defining a frame of reference in which the thermalised CMB $3^0$K radiation is isotropic, that is by removing the dipole component, and the CMB velocity is the velocity of the Earth in that frame. The CMB velocity is a measure of the motion of the solar system relative to the last scattering surface (a spherical shell) of the universe some 13.4Gyrs in the past. The concept here is that at the time of decoupling of this radiation from matter that

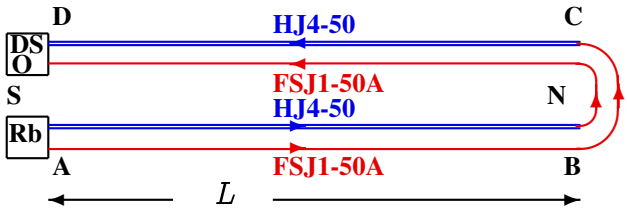


Figure 12: Because Fresnel drag is absent in RF coaxial cables this dual cable setup, using one clock, is capable of detecting the absolute motion of the detector wrt to space, revealing the sidereal rotation effect as well as wave/turbulence effects. In the 1st trial of this detector this arrangement was used, with the cables laid out on a laboratory floor, and results are shown in Figs 6, bottom. In the new design the cables in each circuit are configured into 8 loops, as in Fig.14, giving $L = 8 \times 1.85\text{m} = 14.8\text{m}$. In comparison with data from spacecraft earth-flyby Doppler shifts, Cahill [16], this experiments confirms that there is no Fresnel drag effect in RF coaxial cables. In Cahill [8] a version with optical fibers in place of the HJ4-50 coaxial cables was used, see Fig.18. There the optical fiber has a Fresnel drag effect while the coaxial cable did not. In that experiment optical-electrical converters were used to modulate/demodulate infrared light.

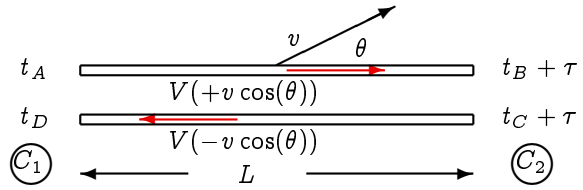


Figure 13: Schematic layout for measuring the one-way speed of EM waves in RF coaxial cables, $V$ is the speed of EM radiation wrt the apparatus, with or without the Fresnel drag and $v$ is the speed of the apparatus through space, in direction $\theta$. Times here refer to absolute times.

matter was on the whole, apart from small observable fluctuations, on average at rest with respect to the 3-space. So the CMB velocity is not motion with respect to the *local* 3-space now; that is the AM velocity. Contributions to the AM velocity would arise from the orbital motion of the solar system within the Milky Way galaxy, which has a speed of some 250 km/s, and contributions from the motion of the Milky Way within the local cluster, and so on to perhaps super clusters, as well as flows of space associated with gravity in the Milky Way and local galactic cluster etc. The difference between the CMB velocity and the AM velocity is explained by the spatial flows that are responsible for gravity at the galactic scales.

# 10 Dual RF Coaxial Cable Detector

The Dual RF Coaxial Cable Detector, Cahill [20] exploits the Fresnel drag anomaly, in that there is no Fresnel drag effect in RF coaxial cables, at low enough frequencies, see Fig.12.

Fig.13 shows the arrangement for measuring the one-way

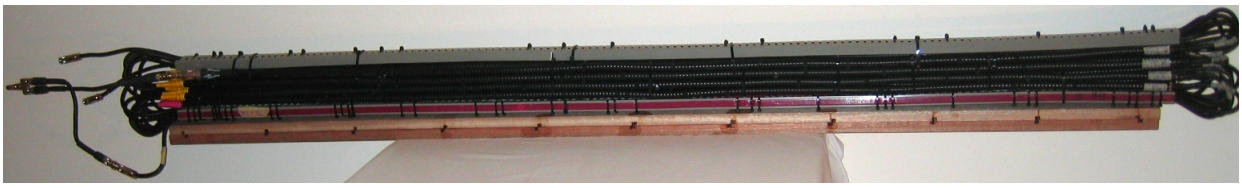

Figure 14: Photograph of the RF coaxial cables arrangement, based upon 16 ×1.85m lengths of phase stabilised Andrew HJ4-50 coaxial cable. These are joined to 16 lengths of phase stabilised Andrew FSJ1-50A cable, in the manner shown schematically in Fig.12. The 16 HJ4-50 coaxial cables have been tightly bound into a 4×4 array, so that the cables, locally, have the same temperature, with cables in one of the circuits embedded between cables in the 2nd circuit. This arrangement of the cables permits the cancellation of temperature differential effects in the cables. A similar array of the smaller diameter FSJ1-50A cables is located inside the grey-coloured conduit boxes.

speed EM waves in RF coaxial cable. The actual travel time $t_{AB}$ from $A$ to $B$ is determined by

$$V(v\cos(\theta))t_{AB} = L + v\cos(\theta)t_{AB} \tag{51}$$

where the 2nd term comes from the end $B$ moving an additional distance $v\cos(\theta)t_{AB}$ during time interval $t_{AB}$. Then

$$t_{AB} = \frac{L}{V(v\cos(\theta)) - v\cos(\theta)} = \frac{nL}{c} + \frac{v\cos(\theta)L}{c^2} + .. \tag{52}$$

$$t_{CD} = \frac{L}{V(v\cos(\theta)) + v\cos(\theta)} = \frac{nL}{c} - \frac{v\cos(\theta)L}{c^2} + .. \tag{53}$$

on using the Fresnel effect, and expanding to 1st oder in $v/c$. However if there is no Fresnel drag effect then we obtain

$$t_{AB} = \frac{L}{V(v\cos(\theta)) - v\cos(\theta)} = \frac{nL}{c} + \frac{v\cos(\theta)Ln^2}{c^2} + .. \tag{54}$$

$$t_{CD} = \frac{L}{V(v\cos(\theta)) + v\cos(\theta)} = \frac{nL}{c} - \frac{v\cos(\theta)Ln^2}{c^2} + .. \tag{55}$$

The important observation is that the $v/c$ terms are independent of the dielectric refractive index $n$ in (52) and (53), but have an $n^2$ dependence in (54) and (55), in the absence of the Fresnel drag effect. Then from (54) and (55) the round trip travel time is, see Fig.12,

$$t_{AB} + t_{CD} = \frac{(n_1 + n_2)L}{c} + \frac{v\cos(\theta)L(n_1^2 - n_2^2)}{c^2} + .. \tag{56}$$

where $n_1$ and $n_2$ are the effective refractive indices for the two different RF coaxial cables, with two separate circuits to reduce temperature effects. Shown in Fig.14 is a photograph. The Andrews Phase Stabilised FSJ1-50A has $n_1 = 1.19$, while the HJ4-50 has $n_2 = 1.11$. One measures the travel time difference of two RF 10MHz signals from a Rubidium frequency standard (Rb) with a Digital Storage Oscilloscope (DSO). In each circuit the RF signal travels one-way in one type of coaxial cable, and returns via a different kind of coaxial cable. Two circuits are used so that temperature effects cancel - if a temperature change alters the speed in one type of cable, and so the travel time, that travel time change is the same in both circuits, and cancels in the difference. The travel time difference of the two circuits at the DSO is

$$\Delta t = \frac{2v\cos(\theta)L(n_1^2 - n_2^2)}{c^2} + .. \tag{57}$$

If the Fresnel drag effect occurred in RF coaxial cables, we would use (54) and (55) instead, and then the $n_1^2 - n_2^2$ term is replaced by 0, i.e. there is no 1st order term in $v$.

The preliminary layout for this detector used cables laid out as in Fig.12, and the data is shown in Fig.6. In the compact design the Andrew HJ4-50 cables are cut into $8 \times 1.85$m shorter lengths in each circuit, corresponding to a net length of $L = 8 \times 1.85 = 14.8$m, and the Andrew FSJ1-50A cables are also cut, but into longer lengths to enable joining. However the curved parts of the Andrew FSJ1-50A cables contribute only at 2nd order in $v/c$. The apparatus was horizontal and orientated NS, and used the rotation of the earth to change the angle $\theta$. The dynamic range of $\cos(\theta)$, caused by the earth rotation only, is again $2\sin(\lambda)\cos(\delta)$, where $\lambda = -35^\circ$ is the latitude of Adelaide. Inclining the detector at angle $\lambda$ removes the earth rotation effect, as now the detector arm is parallel to the earth's spin axis, permitting a more accurate characterisation of the wave effects.

The cable travel times and the DSO phase measurements still have a temperature dependence, and these effects are removed from the data, rather than attempt to maintain a constant temperature, which is impractical because of the heat output of the Rb clock and DSO. The detector was located in a closed room in which the temperature changed slowly over many days, with variations originating from changing external weather driven temperature changes. The temperature of the detector was measured, and it was assumed that the timing errors were proportional to changes in that one measured temperature. These timing errors were some 30ps, compared to the true signal of some 8ps. Because the temperature timing errors are much larger, the temperature induced $\Delta t = a + b\Delta T$ was fitted to the timing data, and the coefficients $a$ and $b$ determined. Then this $\Delta t$ time series was subtracted from the data, leaving the actual required phase data. This is particularly effective as the temperature variations had

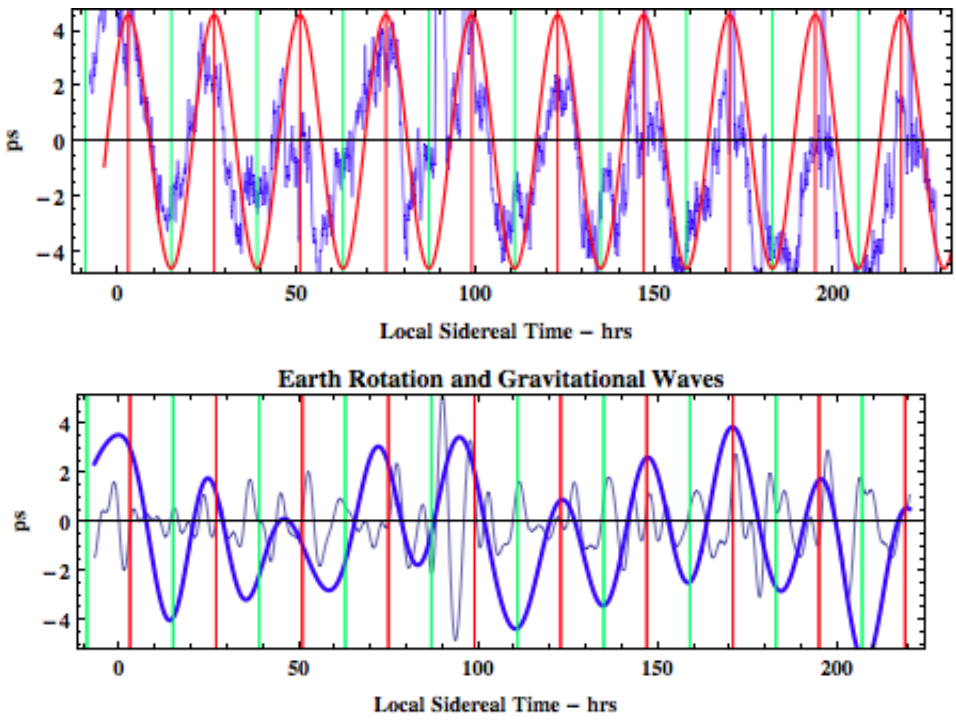


Figure 15: Top: Travel time differences (ps) between the two coaxial cable circuits in Fig.12, orientated NS and horizontal, over 9 days (March 4-12, 2012, Adelaide) plotted against local sidereal time. Sinewave, with dynamic range 8.03ps, is prediction for sidereal effect from flyby Doppler shift data for RA=2.75$^h$ (shown by vertical fudicial lines), Dec=-76.6°, and with speed 499.2km/s, see Table 1. Data shows sidereal effect and significant wave/turbulence effects. Bottom: Data filtered into two frequency bands $3.4 \times 10^{-3}$mHz $< f <$ 0.018mHz ($81.4h > T > 15.3h$) and 0.018mHz $< f <$ 0.067mHz ($15.3h > T > 4.14h$), showing more clearly the earth rotation sidereal effect (plus very low frequency waves) and the turbulence without the sidereal effect. Frequency spectrum of top data is shown in Fig.16.

a distinctive time signature.

The phase data, after removing the temperature effects, is shown in Fig.15 (top), with the data compared with predictions for the sidereal effect only from the flyby Doppler shift data. As well that data is separated into two frequency bands (bottom), so that the sidereal effect is partially separated from the gravitational wave effect, *viz* 3-space wave turbulence. Being 1st order in $v/c$ it is easily determined that the space flow is from the southerly direction. (Miller, 1933) reported the same sense, i.e. the flow is essentially from S to N, though using a 2nd order detector that is more difficult to determine. The frequency spectrum of this data is shown in Fig.16, revealing a fractal $1/f$ form. This implies the fractal structure of the 3-space indicated in Fig.17.

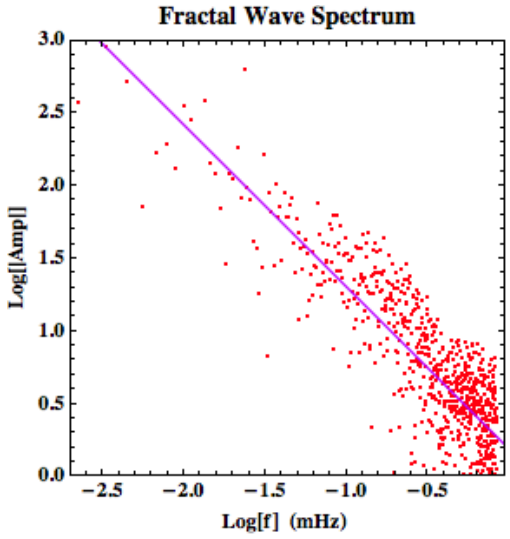


Figure 16: Log-Log plot of the data (top) in Fig.15, with the straight line being $A \propto 1/f$, indicating a $1/f$ fractal wave spectrum. The interpretation for this is the 3-space structure shown in Fig.17.

## 11 Optical Fiber RF Coaxial Cable Detector

An earlier 1st order in $v/c$ gravitational wave detector design is shown in Fig.18, Cahill [8, 9], with some data shown in Fig.19. Only now is it known why that detector also worked, namely that there is a Fresnel drag effect in the optical fibers,

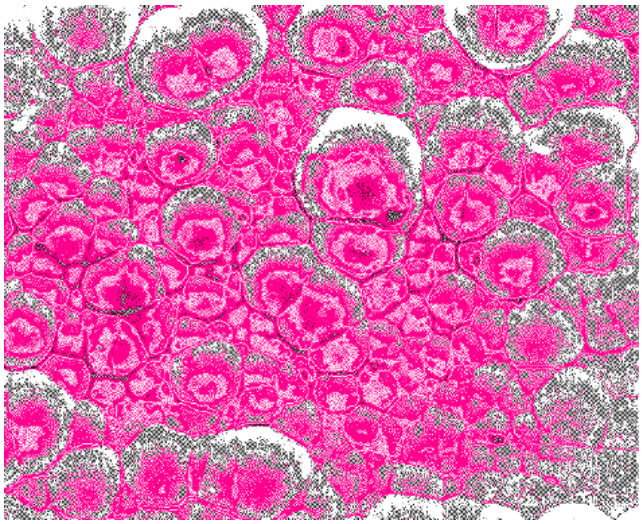

Figure 17: Representation of the fractal wave data as a revealing the fractal textured structure of the 3-space, with cells of space having slightly different velocities, and continually changing, and moving wrt the earth with a speed of ∼500km/s.

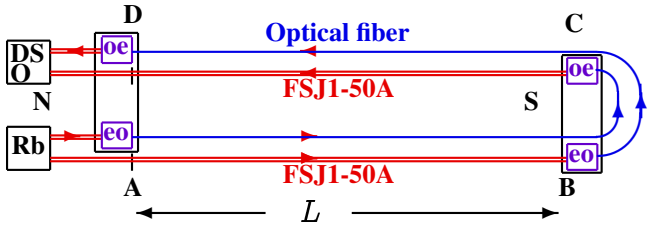


Figure 18: Layout of the optical fiber - coaxial cable detector, with L=5.0m. 10MHz RF signals come from the Rubidium atomic clock (Rb). The Electrical to Optical converters (EO) use the RF signals to modulate 1.3$\mu$m infrared signals that propagate through the single-mode optical fibers. The Optical to Electrical converters (OE) demodulate that signal and give the two RF signals that finally reach the Digital Storage Oscilloscope (DSO), which measures their phase difference. The key effects are that the propagation speeds through the coaxial cables and optical fibers respond differently to their absolute motion through space, with no Fresnel drag in the coaxial cables, and Fresnel drag effect in the optical fibers. Without this key difference this detector does not work.

but not in the RF coaxial cable. Then the travel time difference, measured at the DSO, is given by

$$\Delta t = \frac{2v\cos(\theta)L(n_1^2-1)}{c^2} + .. \qquad (58)$$

where $n_1$ is the effective refractive index of the RF coaxial cable. Again the data is in remarkable agreement with the flyby and other detections of $\mathbf{v}$.

The Dual RF Coaxial Cable Detector exploits the Fresnel drag anomaly in RF coaxial cables, *viz* the drag effect is absent in such cables, for reasons unknown, and this 1st order in $v/c$ detector is compact, robust and uses one clock. This anomaly now explains the operation of the Optical-Fiber - Coaxial Cable Detector, and permits a new calibration. These detectors have confirmed the absolute motion of the solar system and the gravitational wave effects seen in the earlier experiments of Michelson-Morley, Miller, DeWitte. Most significantly these experiments agree with one another, and with the absolute motion velocity vector determined from spacecraft earth-flyby Doppler shifts. The observed significant wave/turbulence effects reveal that the so-called "gravitational waves" are easily detectable in small-scale laboratory detectors, and are considerably larger than those predicted by GR. These effects are not detectable in vacuum-mode Michelson terrestrial interferometers, nor by their analogue vacuum-mode resonant cavity experiments.

The Dual RF Coaxial Cable Detector permits a detailed study and characterisation of the wave effects, and with the detector having the inclination equal to the local latitude the earth rotation effect may be removed, as the detector is then parallel to the earth's spin axis, enabling a more accurate characterisation of the wave effects. The major discovery arising from these various results is that 3-space is directly detectable and has a fractal textured structure. This and numerous other effects are consistent with the dynamical theory for this 3-space. We are seeing the emergence of fundamentally new physics, with space being a a non-geometrical dynamical system, and fractal down to the smallest scales describable by a classical velocity field, and below that by quantum foam dynamics Cahill [6].

## 12 Quantum Zener Diode Detectors

When extending the Dual RF Coaxial Cable Detector experiment to include one located in London, in addition to that located in Adelaide, an analysis of the measured DSO internal noise in each identically setup instrument was undertaken, when the extensive RF coaxial cable array was replaced by short leads. This was intended to determine the S/N ratio for the joint Adelaide-London experiment. Surprisingly the internal noise was found to be correlated, with the noise in the London DSO being some 13 to 20 seconds behind the Adelaide DSO* noise , see Fig.20. The correlation data had a phase that tracked sidereal time, meaning that the average direction was approximately fixed wrt the galaxy, but with extensive fluctuations as well from the gravitational wave/turbulence effect, that had been seen in all previous experiments. The explanation for this DSO effect was not possible as the DSO is a complex instruments, and which component was responding to the passing space fluctuations could

*LeCroy WaveRunner 6051A DSOs were used.

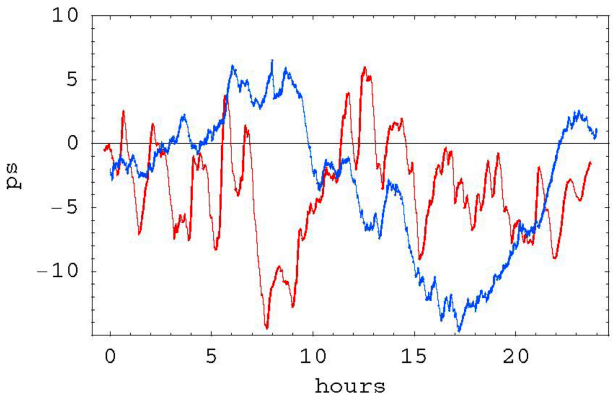


Figure 19: Phase difference (ps), with arbitrary zero, versus local time data plots from the Optical Fiber - Coaxial Cable Detector, see Fig.18 and Cahill [8, 9], showing the sidereal time effect and significant wave/turbulence effects.. The plot with the most easily identified minimum at ∼17 hrs local Adelaide time is from June 9, 2006, while the other plot with the minimum at ∼8.5hrs local time is from August 23, 2006. We see that the minimum has moved forward in time by approximately 8.5 hrs. The expected sidereal shift for this 65 day difference, without wave effects, is 4.3 hrs, to which must be added another ∼1h from the aberration effects shown in Fig11, giving 5.3hrs, in agreement with the data, considering that on individual days the min/max fluctuates by ±2hrs. This sidereal time shift is a critical test for the detector. From the flyby Doppler data we have for August RA=$5^h$, Dec=-70°, and speed 478km/s, giving a predicted sidereal effect dynamic range to be 8.6ps, very close to that observed.

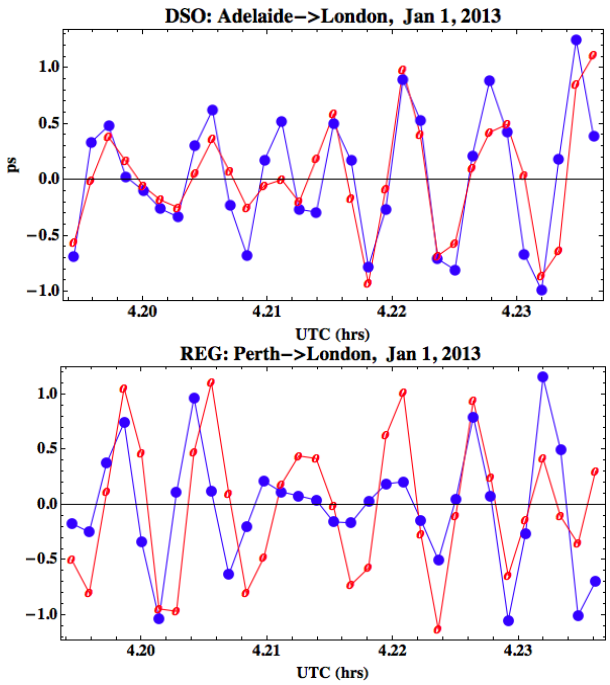


Figure 20: Correlations in band-passed Adelaide-London DSO data (top) and Perth (Australia)-London REG data (bottom), for January 1, 2013, with London data (open dots) advanced by 15s in both cases, over the same 200s time interval. The data points are at 5s intervals. The REG data was recorded every 1s, and has been averaged to 5s intervals for ease of comparison with DSO data. The UTC time at all detectors was determined using internet timing applications, which have ms precision.

not be determined. But the correlation analysis did demonstrate that not all of the internal noise in the DSO was being caused solely by some random process intrinsic to the instrument. Subsequent experiments, below, now suggest that there are zener diodes within the time difference measurements hardware within the DSO.

The travel time delay $\tau(t)$ was determined by computing the correlation function

$$C(\tau,t) = \int_{t-T}^{t+T} dt' S_1(t'-\tau/2) S_2[t'+\tau/2) e^{-a(t'-t)^2} \quad (59)$$

for the two detector signals $S_1(t)$ and $S_2(t)$. Here $2T = 200s$ is the time interval used, about UTC time $t$. The gaussian term ensures the absence of end-effects. Maximising $C(\tau,t)$ wrt $\tau$ gives $\tau(t)$ - the delay time vs UTC $t$, and plotted in Figs. 21 and 22, where the data has been binned into 1hr time intervals, and the rms also shown. The speed and direction, over a 24hr period, was determined by fitting the time delay data using

$$\tau = \frac{\mathbf{R}\cdot\mathbf{v}}{\mathbf{v}^2}, \quad (60)$$

where $\mathbf{R}$ is the Adelaide-London spatial separation vector, and $\mathbf{v}(\theta,\delta)$ is the 3-space velocity vector, parametrised by a speed, RA and Declination. This expression assumes a plane wave form for the gravitational waves. The $\tau(t)$ delay times show large fluctuations, corresponding to fluctuations in speed and/or direction, as also seen in the data in Fig.4, and also a quasi-periodicity, as seen in Fig.20. Then only minimal travel times, $10s < \tau < 22s$, were retained. Correlations, as shown in Fig.20, are not always evident, and then the correlation function $C(\tau,t)$ has a low value. Only $\tau(t)$ data from high values of the correlation function were used. The absence of correlations at all times is expected as the London detector is not directly "downstream" of the Adelaide detector, and so a fractal structure to space, possessing a spatial inhomogeneity, bars ongoing correlations, and as well the wave structure will evolve during the travel time. Fig.20 shows examples of significant correlations in phase and amplitude between all four detectors, but with some mismatches. The approximate travel time of 15s in Fig.20 at ∼4.2hrs UTC is also apparent in Fig.21, with the top figure showing the discovery of the correlations from the two DSO separated by a distance $R \approx 12160$km. That the internal "noise" in these DSO is correlated is a major discovery.

There are much simpler devices that were discovered to also display time delayed correlations over large distances:

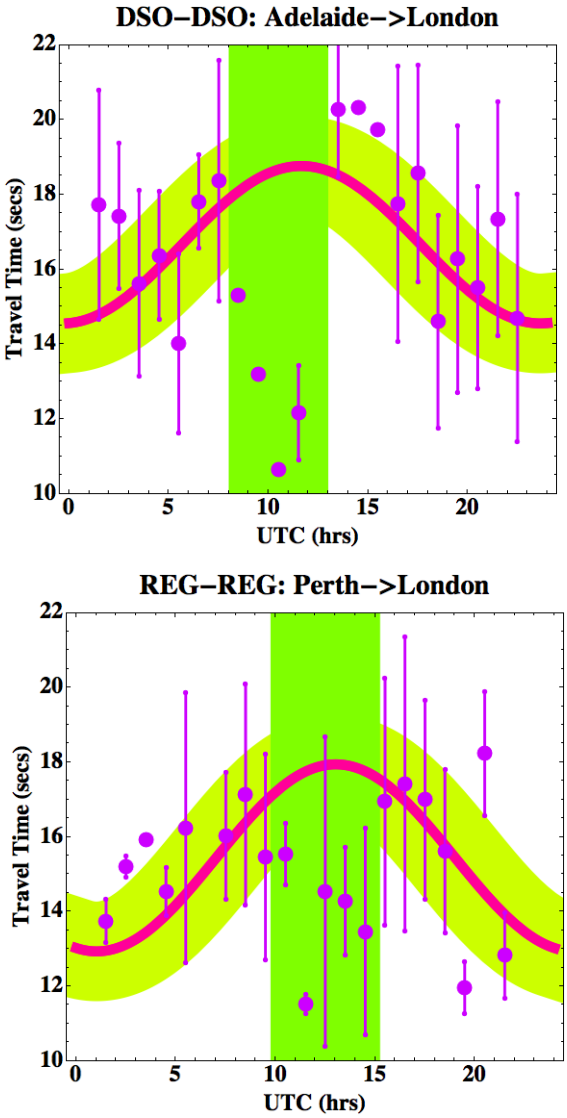


Figure 21: Travel times from DSO-DSO Adelaide-London data (top), and REG-REG Perth-London data (bottom) from correlation analysis using (59). The data in each 1 hr interval has been binned, and the average and rms shown. The thick (red line) shows best fit to data using plane wave travel time predictor, (60), but after excluding those data points between 8 and 13hrs UTC (top) and 10 and 15hrs UTC (bottom), indicated by vertical band. Those data points are not consistent with the plane wave modelling, and suggest a scattering process when the waves pass deeper into the earth, see fig.23. The Perth-London phase is retarded wrt Adelaide-London phase by $\sim$1.5hrs, consistent with Perth being 1.5hrs west of Adelaide. The Adelaide-London data gives speed = 512 km/s, RA = 4.8 hrs, Dec = 83°S, and the Perth-London data gives speed = 528 km/s, RA = 5.3 hrs, Dec = 81°S. The broad band tracking the best fit line is for +/- 1 sec fluctuations, corresponding to speed fluctuation of +/- 17km/s. Actual fluctuations are larger than this, as 1st observed by Michelson-Morley and by Miller, see Fig.4.

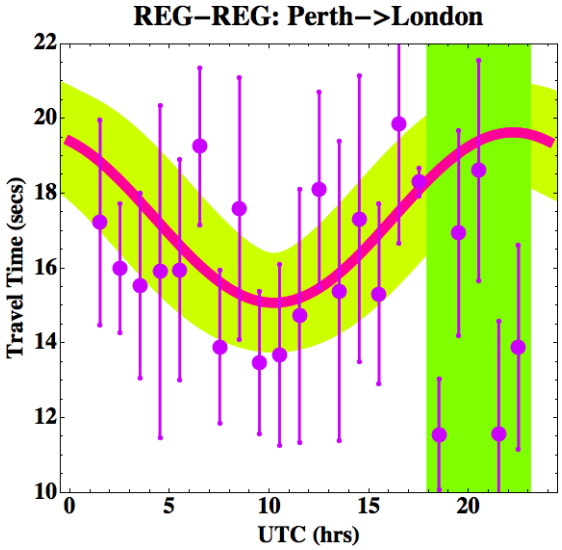


Figure 22: Travel times from REG-REG Perth-London data for August 1, 2012. The data in each 1 hr interval has been binned, and the average and rms shown. The thick line shows best fit to data using plane wave travel time predictor, (60), but after excluding those data points between 18 and 23hrs UTC, indicated by vertical band. Those data points are not consistent with the plane wave modelling. This data gives speed = 471 km/s, RA = 4.4 hrs, Dec = 82°S. The change in phase of the maximum of the data, from UTC= 22+/-2 hr, for August 1, 2012, to UTC = 12+/- 2 hr for January 2013 (Fig.21), but with essentially the same RA, illustrates the sidereal effect: the average direction of the space flow is fixed wrt to the stars, apart from the earth-orbit aberration effect, Fig.11.

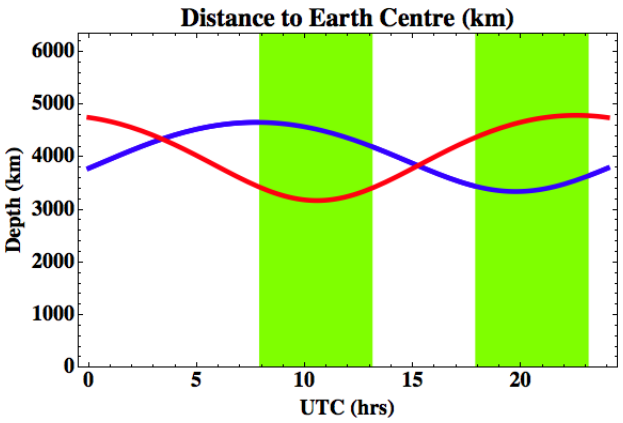


Figure 23: Given measured space velocity, plots show maximum earth penetration depth of space detected by London detectors for Adelaide→London, Jan1, 2013 and Perth→London, August 1, 2012 , revealing that the anomalous scattering occurs when deeper depths are "traversed". The vertical shadings correspond to those in Fig.21 (top) and Fig.22.

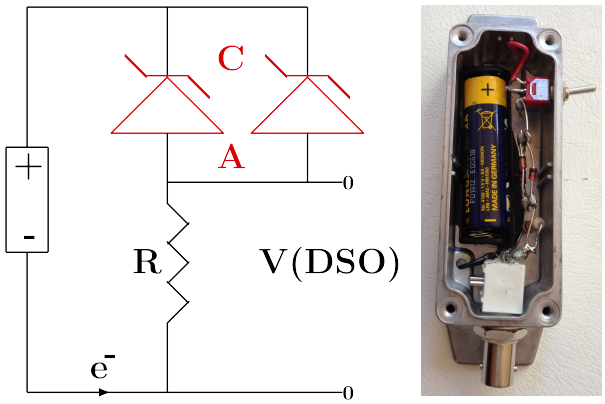


Figure 24: Left: Circuit of Zener Diode Gravitational Wave Detector, showing 1.5V AA battery, two 1N4728A zener diodes operating in reverse bias mode, and having a Zener voltage of 3.3V, and resistor R= 10KΩ. Voltage V across resistor is measured and used to determine the space driven fluctuating tunnelling current through the zener diodes. Correlated currents from two collocated detectors are shown in Fig.25. Right: Photo of detector with 6 zener diodes in parallel.

these are the Random Number Generators (RNG) or Random Event Generators (REG). There are various designs available from manufacturers, and all claim that these devices manifest hardware random quantum processes, as they involve the quantum to classical transition when a measurements, say, of the quantum tunnelling of electrons through a nanotechnology potential barrier, ∼10nm thickness, is measured by a classical/macroscopic system. According to the standard interpretation of the quantum theory, the collapse of the electron wave function to one side or the other of the barrier, after the tunnelling produces a component on each side, is purely a random event, internal to the quantum system. However this interpretation had never been tested experimentally. Guided by the results from the DSO correlated-noise effect, the data from two REGs, located in Perth and London, was examined. The data* showed the same correlation effect as observed in the DSO experiments, see Figs. 20-22. However REGs typically employ a XOR gate that produces integer valued outputs with a predetermined statistical form.

To study the zener diode tunnelling currents without XOR gate intervention two collocated zener diode circuits were used to detect highly correlated tunnelling currents, Figs.24 and 25. When the detectors are separated by ∼0.25m in NS direction, phase differences $\sim 0.5\mu$s were observed and dependent on relative orientation. So this zener diode circuit forms a very simple and cheap nanotechnology quantum detector for gravitational waves.

*The data is from the GCP international network: http://teilhard.globalmind.org/.

# 13 Dynamical 3-Space

If Michelson and Morley had more carefully presented their pioneering data physics would have developed in a very different direction. Even by 1925/26 Miller, a junior colleague of Michelson, was repeating the gas-mode interferometer experiment, and by not using Newtonian mechanics to attempt a calibration of the device, rather by using the earth aberration effect which utilised the earth orbital speed of 30km/s to set the calibration constant, although that also entailed false assumptions. The experimental data reveals the existence of a dynamical space. It is a simple matter to derive the dynamics of space, and the emergence of gravity as a quantum matter effect.

Physics must employ a covariance formulation, in the sense that ultimately predictions are independent of observers, and that there must also be a relativity principle that relates observational data by different observers. We assume then that space has a structure whose movement, wrt an observer, is described by a velocity field, $\mathbf{v}(\mathbf{r}, t)$, at the classical physics level, at a location $\mathbf{r}$ and time $t$, as defined by the observer. In particular the space coordinates $\mathbf{r}$ define an embedding space, which herein we take to be Euclidean. At a deeper level space is probably a fractal quantum foam, which is only approximately embeddable in a 3-dimensional space at a coarse-grained level, Cahill [6, 15, 17]. This embedding space has no ontological existence - it is not real. Ironically Newton took this space to be real but unobservable, and so a different concept, and so excluding the possibility that gravity was caused by an accelerating space. It is assumed that different observers, in relative uniform motion, relate their description of the velocity field by means of the Galilean Relativity Transformation for positions and velocities. It is usually argued that the Galilean Relativity Transformations were made redundant and in error by the Special Relativity Transformations. However this is not so - there exist an exact linear mapping between Galilean Relativity and Special Relativity (SR), differing only by definitions of space and time coordinates Cahill [12, 13]. This implies that the so-called Special Relativity (SR) relativistic effects are not actual dynamical effects - they are purely areifacts of a peculiar choice of space and time coordinates. In particular Lorentz symmetry is merely a consequence of this choice of space and time coordinates, and is equivalent to Galilean symmetry. Nevertheless Lorentz symmetry remains valid, even though a local preferred frame of reference exists. Lorentz Relativity, however, goes beyond Galilean Relativity in that the limiting speed of systems wrt to the local space causes various so-called relativist effects, such as length contractions and clock dilations.

The Euler covariant constituent acceleration $\mathbf{a}(\mathbf{r}, t)$ of space is then defined by

$$\mathbf{a} = \lim_{\Delta t \to 0} \frac{\mathbf{v}(\mathbf{r} + \mathbf{v}(\mathbf{r}, t)\Delta t, t + \Delta t) - \mathbf{v}(\mathbf{r}, t)}{\Delta t}$$

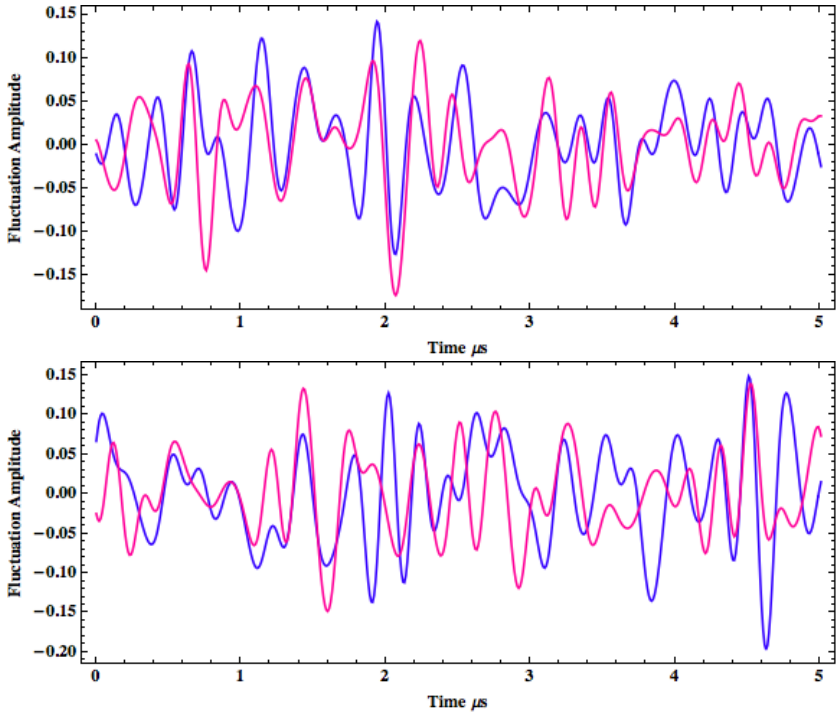


Figure 25: Top: Current fluctuations from two collocated zener diode detectors, Fig.24 (separated by 3-4 cm in EW direction due to box size) , revealing strong correlations. The small separation may explain slight differences, revealing a structure to space at very small distances. Bottom: Correlations when detectors separated NS by approximately 25 cm, and with N detector signal advanced by 0.5 $\mu$s, and then showing strong correlations. This time delay effect reveals space traveling from S to N at a speed of approximately 500km/s. Fig.26 shows plot of correlation function $C(\tau, t)$ with time delay $\tau$ expressed as a speed over a distance of 25 cm.

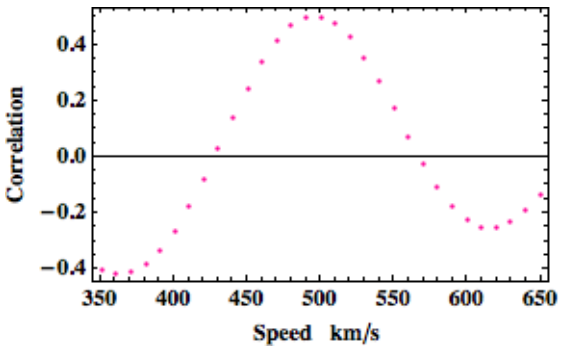


Figure 26: Correlation function $C(\tau, t)$, (59), with time delay $\tau$ expressed as a speed over a distance of 25 cm, for the data shown in Fig.25, Bottom. $t$ is the time of observation, which is not relevant in this test case. This plot reveals a speed of 500$\pm$25 km/s.

$$= \frac{\partial \mathbf{v}}{\partial t} + (\mathbf{v}\cdot\nabla)\mathbf{v}$$

which describes the acceleration of a constituent element of space by tracking its change in velocity. This means that space has a (quantum) structure that permits its velocity to be defined and detected, which experimentally has been done. We assume here that the flow has zero vorticity $\nabla \times \mathbf{v} = \mathbf{0}$, and then the flow is determined by a scalar function $\mathbf{v} = \nabla u$. We then need one scalar equation to determine the space dynamics, which we construct by forming the divergence of $\mathbf{a}$. The inhomogeneous term then determines a dissipative flow caused by matter, expressed as a matter density, and where the coefficient turns out to be Newton's gravitational constant,

$$\nabla\cdot\left(\frac{\partial \mathbf{v}}{\partial t} + (\mathbf{v}\cdot\nabla)\mathbf{v}\right) = -4\pi G\rho(\mathbf{r}, t) \qquad (61)$$

Note that even a time independent matter density or even the absence of matter can be associated with a time-dependent flow. In particular this dynamical space in the absence of matter has an expanding universe solution. Substituting the Hubble form $\mathbf{v}(\mathbf{r}, t) = H(t)\mathbf{r}$, and then using $H(t) = \dot{a}(t)/a(t)$, where $a(t)$ is the scale factor of the universe, we obtain the solution $a(t) = t/t_0$, where $t_0$ is the age of the universe, since

by convention $a(t_0) = 1$. Then computing the magnitude-redshift function $\mu(z)$, we obtain excellent agreement with the supernova red-shift data, Cahill and Rothall [26].

This equation follows essentially from covariance and dimensional analysis. For a spherically symmetric matter distribution, of total mass $M$, and a time-independent spherically symmetric flow we obtain from the above, and external to the sphere of matter, the acceleration of space

$$\mathbf{v}(\mathbf{r}) = -\sqrt{\frac{2GM}{r}}\hat{\mathbf{r}}, \text{ giving } \quad \mathbf{a}(\mathbf{r}) = -\frac{GM}{r^2}\hat{\mathbf{r}} \qquad (62)$$

which is the inverse square law. Newton applied such an acceleration to matter, not space, and which Newton invented directly by examining Kepler's planetary motion laws, but which makes no mention of what is causing the acceleration of matter, although in a letter in 1675 to Oldenburg, Secretary of the Royal Society, and later to Robert Boyle, he speculated that an undetectable ether flow through space may be responsible for gravity. Here, however, the inverse square law emerges from the Euler constituent acceleration, which imposes a space self-interaction. At the surface of the earth the in-flow speed is 11km/s, and the sun in-flow speed at 1AU is 42km/s, with both detected Cahill, [15].

While the above 3-space dynamical equation followed from covariance and dimensional analysis, this derivation is not complete yet. One can add additional terms with the same order in speed and spatial derivatives, and which cannot be *a priori* neglected. These developments have been extensively tested with experiments and observations, Cahill [6, 10, 15, 24], Rothall and Cahill [36, 37] and Cahill and Kerrigan [25].

# 14 Quantum Matter and 3-Space: Emergent Gravity

We now derive, uniquely, how quantum matter responds to the dynamical 3-space. This gives the 1st derivation of the phenomenon of gravity, and reveals this to be a quantum matter wave refraction effect. For a free-fall quantum system with mass $m$ the Schrödinger equation is uniquely generalised, Cahill [11], with the new terms required to maintain that the motion is intrinsically wrt the 3-space, and not wrt the embedding space, and that the time evolution is unitary

$$i\hbar\frac{\partial\psi(\mathbf{r},t)}{\partial t} = -\frac{\hbar^2}{2m}\nabla^2\psi(\mathbf{r},t) - i\hbar\left(\mathbf{v}.\nabla + \frac{1}{2}\nabla.\mathbf{v}\right)\psi(\mathbf{r},t)$$

The space and time coordinates $\{t, x, y, z\}$ ensure that the separation of a deeper and unified process into different classes of phenomena - here a dynamical 3-space (quantum foam) and a quantum matter system, is properly tracked and connected. As well the same coordinates may be used by an observer to also track the different phenomena. A quantum wave packet propagation analysis gives the matter acceleration $\mathbf{g} = d^2<\mathbf{r}>/dt^2$ induced by wave refraction to be

$$\mathbf{g} = \frac{\partial\mathbf{v}}{\partial t} + (\mathbf{v}.\nabla)\mathbf{v} + (\nabla\times\mathbf{v})\times\mathbf{v}_R + ...$$
$$\mathbf{v}_R(\mathbf{r}_0(t),t) = \mathbf{v}_0(t) - \mathbf{v}(\mathbf{r}_0(t),t),$$

where $\mathbf{v}_R$ is the velocity of the wave packet relative to the 3-space, and where $\mathbf{v}_O$ and $\mathbf{r}_O$ are the velocity and position relative to the observer. The last term generates the Lense-Thirring effect as a vorticity driven effect. In the limit of zero vorticity we obtain that the quantum matter acceleration is the same as the 3-space acceleration: $\mathbf{g} = \mathbf{a}$. This confirms that the new physics is in agreement with Galileo's observations that all matter falls with the same acceleration. Using arcane language this amounts to a derivation of the Weak Equivalence Principle.

Significantly the quantum matter 3-space-induced 'gravitational' acceleration also follows from maximising the elapsed proper time wrt the quantum matter wave-packet trajectory $\mathbf{r}_o(t)$, Cahill [7],

$$\tau = \int dt\sqrt{1 - \frac{\mathbf{v}_R^2(\mathbf{r}_0(t),t)}{c^2}} \qquad (63)$$

which entails that matter has a maximum speed of $c$ wrt to space, and not wrt an observer. This maximisation ensures that quantum waves propagating along neighbouring paths are in phase - the condition for a classical trajectory. This gives

$$\mathbf{g} = \frac{\partial\mathbf{v}}{\partial t} + (\mathbf{v}\cdot\nabla)\mathbf{v} + (\nabla\times\mathbf{v})\times\mathbf{v}_R$$
$$-\frac{\mathbf{v}_R}{1-\frac{\mathbf{v}_R^2}{c^2}}\frac{1}{2}\frac{d}{dt}\left(\frac{\mathbf{v}_R^2}{c^2}\right) + ... \qquad (64)$$

and then taking the limit $v_R/c \to 0$ we recover the non-relativistic limit, above. This shows that (i) the matter 'gravitational' geodesic is a quantum wave refraction effect, with the trajectory determined by a Fermat maximum proper-time principle, and (ii) that quantum systems undergo a local time dilation effect. The last, relativistic, term generates the planetary precession effect. If clocks are forced to travel different trajectories then the above predicts different evolved times when they again meet - this is the Twin Effect, which now has a simple and explicit physical explanation - it is an absolute motion effect, meaning motion wrt space itself. This elapsed proper time expression invokes Lorentzian relativity, that the maximum speed is $c$ wrt to space, and not wrt the observer, as in Einstein SR. The differential proper time (63) has the form

$$c^2d\tau^2 = c^2dt^2 - (d\mathbf{r} - \mathbf{v}(\mathbf{r},t)dt)^2 = g_{\mu\nu}dx^\mu dx^\nu$$

which defines an induced metric for a curved spacetime manifold. However this has no ontological significance, and the metric is not determined by GR.

# 15 Electromagnetic Radiation and Dynamical Space

We must generalise the Maxwell equations so that the electric and magnetic fields are excitations within the dynamical 3-space, and not of the embedding space. The minimal form in the absence of charges and currents is

$$\begin{aligned} \nabla \times \mathbf{E} &= -\mu_0 \left( \frac{\partial \mathbf{H}}{\partial t} + \mathbf{v}.\nabla \mathbf{H} \right), \quad \nabla.\mathbf{E} = \mathbf{0}, \\ \nabla \times \mathbf{H} &= \epsilon_0 \left( \frac{\partial \mathbf{E}}{\partial t} + \mathbf{v}.\nabla \mathbf{E} \right), \quad \nabla.\mathbf{H} = \mathbf{0} \end{aligned}$$

which was first suggested by Hertz [29], but with $\mathbf{v}$ then being only a constant vector field, and not interpreted as a moving space effect. As easily determined the speed of EM radiation is now $c = 1/\sqrt{\mu_0 \epsilon_0}$ with respect to the 3-space, and not wrt an observer in motion through the 3-space. The Michelson-Morley 1887 experiment 1st detected this anisotropy effect, as have numerous subsequent experiments. A time-dependent and/or inhomogeneous velocity field causes the refraction of EM radiation. This can be computed by using the Fermat least-time approximation - the opposite of that for quantum matter. This ensures that EM waves along neighbouring paths are in phase. Then an EM ray path $\mathbf{r}(t)$ is determined by minimising the elapsed travel time:

$$T = \int_{s_i}^{s_f} \frac{ds |\frac{d\mathbf{r}}{ds}|}{|c\hat{\mathbf{v}}_R(s) + \mathbf{v}(\mathbf{r}(\mathbf{s}), \mathbf{t}(\mathbf{s})|},$$

with $\mathbf{v}_R = \frac{d\mathbf{r}}{dt} - \mathbf{v}(\mathbf{r}(\mathbf{t}), \mathbf{t})$, by varying both $\mathbf{r}(s)$ and $t(s)$, finally giving $\mathbf{r}(t)$. Here $s$ is an arbitrary path parameter, and $c\hat{\mathbf{v}}_R$ is the velocity of the EM radiation wrt the local 3-space, namely $c$. The denominator is the speed of the EM radiation wrt the observer's Euclidean spatial coordinates. This equation may also be used to calculate the gravitational lensing by black holes, filaments, Cahill [18], and by ordinary matter, using the appropriate 3-space velocity field. It produces the measured light bending by the sun.

# 16 Conclusions

Herein is reviewed extensive experimental evidence that a dynamical 3-space is the foundation process of reality and, in particular, that the speed of light is not invariant, as claimed in the spacetime theory that has dominated academic physics since 1905. This dynamical space passes the earth with a speed ∼500km/s from a near southerly direction, and the first detection of that is now understood to go back to the Michelson-Morley experiment of 1887, now that it is understood that the original report in 1887 was flawed by a lack of understanding of how the interferometer should have been calibrated. That misunderstanding led to the development of the spacetime model. More recently a variety of experimental techniques have been developed, with the latest using the Zener diode quantum detectors, that permit the detection of this space, which the data shows has a fractal structure. The theory for this dynamical space has been found by generalising Newtonian gravity by first converting that to a velocity field formalism, which then immediately permitted a generalisation that did not alter the inverse square law outside of spherically symmetric masses. This dynamical theory has permitted the resolution of numerous anomalies in physics, $g$ decreasing more slowly down boreholes than predicted by NG or GR, inconsistent laboratory measurements of $G$, flat rotation plots for spiral galaxies, star dynamics near the centre of the Milky Way central black hole, effects of a earth centred black hole, which causes the $g$ anomaly, and its effect on the generation of matter within the earth via intense 3-space fluctuations [19]. [25], cosmic filaments [18] and networks of black holes connected by cosmic filaments [36], uniformly expanding universe [26] without the need for 'dark matter' nor 'dark energy', which were merely fix-ups for General Relativity, which failed to explain any of the above anomalies. Determination of location in space and in time requires the use of no-Lorentz Relativity, and involves correction for the effects of absolute motion through space upon clocks and rods. Generalising the quantum theory to include this dynamical space led to gravity being an emergent quantum phenomenon, being caused by the refraction of quantum matter waves by the dynamical space: the unification of gravity and quantum physics. The dynamical space theory has no measure of energy or energy content, contrary to the usual Zero Point Energy notion, but its interaction with quantum matter generates energy; this is the violation of the conservation of energy principle, and had previously been discovered by N. Tesla, T.T. Brown, W. Reich, T.H. Moray, and others. This effect is the basis for the Zener diode quantum detection of the dynamical space, and also correlations between dynamical space fluctuations and Solar flare rates, which leads to a new explanation of the correlation between Solar flare counts and the Earth's climate [27], and also the anisotropic Brownian motion of colloidal particle droplets in water [28]. We note that dynamical 3-space is not an aether substance in a inactive geometrical space, but a complex quantum dynamical system, which at a sufficiently large scale permits a geometrical and velocity field description [6], and with quantum behaviour arising from a pattern recognising activity within a neural network like system, with such patterns being semantic information within that system.

A specials thank you to Martin Kokus for organising the NPA meeting in Baltimore in 2014.

# References


[1] Anderson J.D., Campbell J.K., Ekelund J.E., Ellis J. and Jordan J.F. Anomalous Orbital-Energy Changes Observed during Spacecraft Flybys

[2] Brown H.R. The Origins of Length Contraction; I The Fitzgerald-Lorentz Deformation Hypothesis, Am. J. Phys., v. 69, 1044-1054 (2001).

[3] Brown H.R. Physical Relativity: Space-Time Structure from a Dynamical Perspective, Clarendon Press Oxford (2005).

[4] Brown H.R. and Pooley O. Minkowski Space-Time: a Glorious Non-Entity, in The Ontology of Spacetime, Dieks, ed. Elsevier, 67-89 (2006).

[5] Cahill R.T. and Kitto K. Michelson-Morley Experiments Revisited, Apeiron, 10(2),104-117 (2003).

[6] Cahill R.T. Process Physics: From Information Theory to Quantum Space and Matter, Nova. Sci. Pub. NY (2005).

[7] Cahill R.T. The Michelson and Morley 1887 Experiment and the Discovery of Absolute Motion, Progress in Physics, 3, 25-29, (2005).

[8] Cahill R.T. A New Light-Speed Anisotropy Experiment: Absolute Motion and Gravitational Waves Detected, Progress in Physics, 4, 73-92 (2006).

[9] Cahill R.T. Absolute Motion and Gravitational Wave Experiment Results, Contribution to Australian Institute of Physics National Congress, Brisbane, Paper No. 202 (2006).

[10] Cahill R.T. 3-Space Inflow Theory of Gravity: Boreholes, Black holes and the Fine Structure Constant, Progress in Physics, 2, 9-16 (2006).

[11] Cahill R.T. Dynamical Fractal 3-Space and the Generalised Schrödinger Equation: Equivalence Principle and Vorticity Effects, Progress in Physics, 1, 27-34 (2006).

[12] Cahill R.T. The Roland De Witte 1991 Experiment, Progress in Physics, 3, 60-65 (2006).

[13] Cahill R.T. Unravelling Lorentz Covariance and the Space-time Formalism, Progress in Physics, 4, 19-24 (2008).

[14] Cahill R.T. The Dynamical Velocity Superposition Effect in the Quantum-Foam Theory of Gravity, in Relativity, Gravitation, Cosmology: New Developments, Dvoeglazov V., ed., Nova Science Pub., New York (2009).

[15] Cahill R.T. Dynamical 3-Space: A Review, in Ether Space-time and Cosmology: New Insights into a Key Physical Medium, Duffy and Levy, eds., Apeiron, 135-200 (2009).

[16] Cahill R.T. Combining NASA/JPL One-Way Optical-Fiber Light Speed Data with Spacecraft Earth-Flyby Doppler-Shift Data to Characterise 3-Space Flow, Progress in Physics, 4, 50-64 (2009).

[17] Cahill R.T. Dynamical 3-Space: Emergent Gravity, in Should the Laws of Gravity be Reconsidered? Munera, H.A., ed., Apeiron, Montreal, 363-376 (2011).

[18] Cahill R.T. Dynamical 3-Space: Cosmic Filaments, Sheets and Voids, Progress in Physics, 2, 44-51 (2011).

[19] Cahill R.T. Dynamical 3-Space and the Earth's Black Hole :An Expanding Earth Mechanism. In G Scalera, E Boschi and S Cwojdziński, eds. The Earth Expansion Evidence - A Challenge for Geology, Geophysics and Astronomy. 1 ed. Rome, Italy: ARACNE editrice. 37th Workshop of the International School of Geophysics. Erice, Italy 2011, 185-196 (2012).

[20] Cahill R.T. Characterisation of Low Frequency Gravitational Waves from Dual RF Coaxial-Cable Detector: Fractal Textured Dynamical 3-Space, Progress in Physics, 3, 3-10, (2012).

[21] Cahill R.T. One-Way Speed of Light Measurements Without Clock Synchronisation, Progress in Physics, 3, 43-45 (2012).

[22] Cahill R.T. Dynamical 3-Space: Neo-Lorentz Relativity, Physics International 4(1), 60-72. doi:10.3844/pisp.2013.60.72 Published Online 4 (1) (http://www.thescipub.com/pi.toc) (2013).

[23] Cahill R.T. Nanotechnology Quantum Detectors for Gravitational Waves: Adelaide to London Correlations Observed, Progress in Physics, 4, 57-62 (2013).

[24] Cahill R.T. Discovery of Dynamical 3-Space: Theory, Experiments and Observations - A Review, American Journal of Space Science, doi:10.3844 /ajssp.2013.77.93 Published Online 1(2) (http://www.thescipub.com/ajss.toc) (2013).

[25] Cahill R.T. and Kerrigan D. Dynamical Space: Supermassive Black Holes and Cosmic Filaments, Progress in Physics 4, 79-82 (2011).

[26] Cahill R.T. and Rothall D. Discovery of Uniformly Expanding Universe, Progress in Physics, 1, 63-68 (2012).

[27] Cahill R.T. Solar Flare Five-Day Predictions from Quantum Detectors of Dynamical Space Fractal Flow Turbulence: Gravitational Wave Diminution and Earth Climate Cooling, Progress in Physics, v.10, 236-242 (2014).

[28] Cahill R.T. Dynamical 3-Space: Energy NonConservation, Anisotropic Brownian Motion Experiment and Ocean Temperatures, viXra, (2015).

[29] Hertz H. On the Fundamental Equations of Electro-Magnetics for Bodies in Motion, Wiedemann's Ann. 41, 369; (1890). Electric Waves, Collection of Scientific Papers, Dover Pub., New York (1962).

[30] Lorentz H.A. Electromagnetic Phenomena in System Moving with any Velocity Smaller than that of Light , Proc. of the Royal Netherlands Academy of Arts and Sciences, v. 6, 809-831 (1904).

[31] Lorentz H.A. De relatieve beweging van de aarde en den aether, Amsterdam, Zittingsverlag Akad. v. Wet., 1, p. 74-79, (transl.: The relative motion of the earth and the aether) (1892).

[32] Fitzgerald G.F. The Ether and the Earth's Atmosphere, Science, v. 13, 390 (1889).

[33] Michelson A.A. and Morley E.W. On the Relative Motion of the Earth and the Luminiferous Ether, Am. J. Sc. 34, 333-345 (1887).

[34] Miller D.C. The Ether-Drift Experiment and the Determination of the Absolute Motion of the Earth, Rev. Mod. Phys., 5, 203-242 (1933).

[35] Pound R.V. and Rebka Jr. G.A. Apparent Weight of Photons, Phys. Rev. Lett., 4(7), 337-341 (1960).

[36] Rothall D.P. and Cahill R.T. Dynamical 3-Space: Black Holes in an Expanding Universe, Progress in Physics, 4, 25-31 (2013).

[37] Rothall D.P. and Cahill R.T. Dynamical 3-Space: Observing Gravitational Wave Fluctuations and the Shnoll Effect using a Zener Diode Quantum Detector, Progress in Physics, 10 (1), 16-18 (2014).